Shared Slides for High-Latitude I-T Processes

Thursday 10:00-12:00, Mesa C/Hilton

http://cedarweb.vsp.ucar.edu/wiki/index.php/2019_Workshop:High_latitude_IT_processes

Schedule

Presenter	Title
Jiang Liu	Dawn side auroral polarization streams
Larry Lyons	Flow channel control of substorm azimuthal expansion
Russell Landry	Storm-time DMSP Poynting flux measurements and conductance estimations
Michael Negale	Tracking Polar Cap Patches Using a Reconstructed Ionosphere
Joaquin Diaz-Pena	Polar cap boundary dynamics
Zihan Wang	Observation and modeling of polar cap patches
Ying Zou	Effect of substorms on upper thermospheric winds
Olga Verkhoglyadova	Importance of Magnetosphere-Ionosphere-Thermosphere coupling at meso- and small-scales
Doga Ozturk	Modeling meso-scale electric field variability through GCMs
Qingyu Zhu	Impact of binning methods on high-lat electrodynamic forcing
Ildiko Horvath/Cheryl Huang	MIT coupling captured by OpenGGCM
Meghan Burleigh	Ion outflow, model and rocket data
Rachel Frissell/Andy Gerrard	NJIT AGOs
Ashton Reimer	New RISR capability
Nathaniel Frissell	Antarctic HF receiver
Alex Chartier/Ethan Miller	RadioICE: A new HF ionospheric sounder in Antarctica

Jiang Liu, UCLA

Dawnside Auroral Polarization Stream (DAPS)

Jiang Liu, L. R. Lyons, Chih-Ping Wang, et al., UCLA

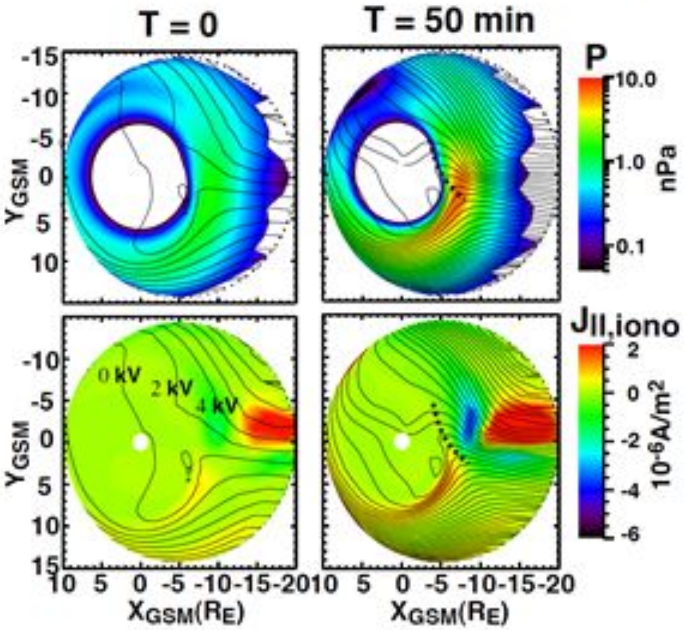

Gkioulidou et al., (2009)

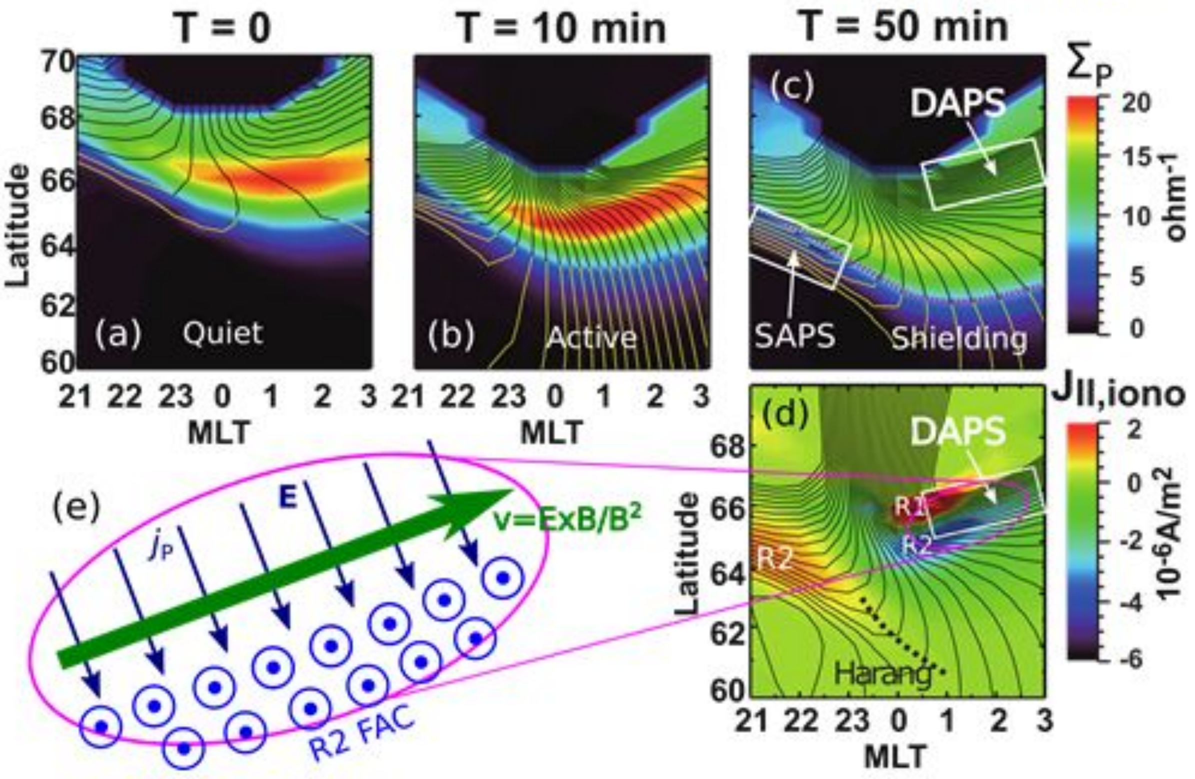

- From T=0 min to T=50 min: Convection keeps enhancing.

DAPS Examples

- Two events in the post-midnight sector.
- Bright arc indicates that the R2 current is enhanced.
- Bottom event:
  - The DAPS is immediately poleward of an Omega band's bright arc [Liu et al. 2018 (2017GL076485)].
    - Omega bands are the most significant auroral structure in the post-midnight to dawn sector—they cause ~1000 nT of geomagnetic perturbation.
  - The DAPS's magnetospheric counterpart may trigger an instability to produce the Omega bands.

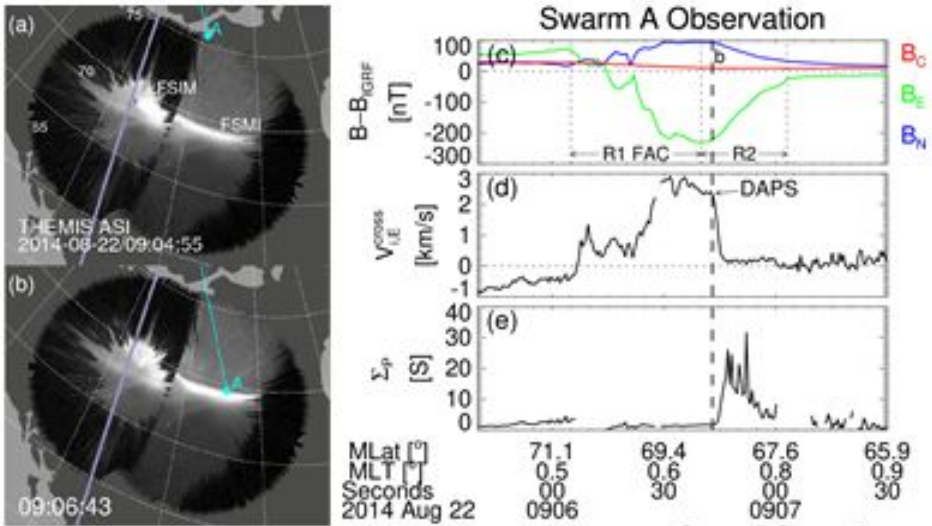

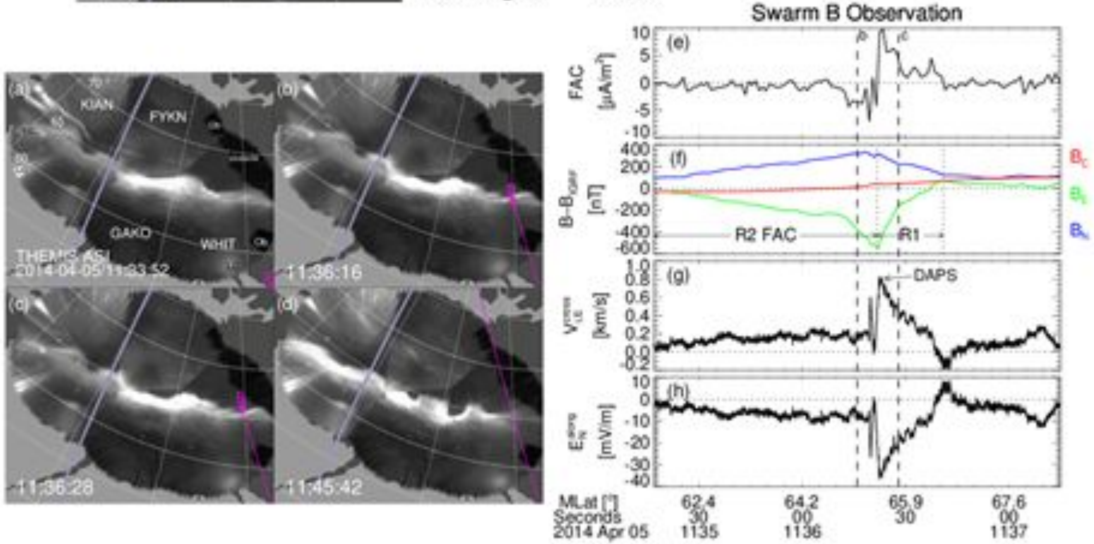

Open Questions

- Under what conditions is DAPS strong?
- Is conductivity gradient necessary for the steep flow gradient of DAPS?
- How does DAPS differ from the background convection?

Larry Lyons, UCLA

FLOW CHANNEL DRIVEN ENHANCEMENT OF SAPS AND DAPS, AND CONTROL OF SUBSTORM ONSET AND ITS LONGITUDINAL EXPANSION

L. R. Lyons, J. Liu, Y. Nishimura, A. S. Reimer, D. L. Hampton, C.-P. Wang, W. A. Bristow, B. Gallardo-Lacourt, X. Shi, R. H. Varney, V. Angelopoulos, and E. F. Donovan

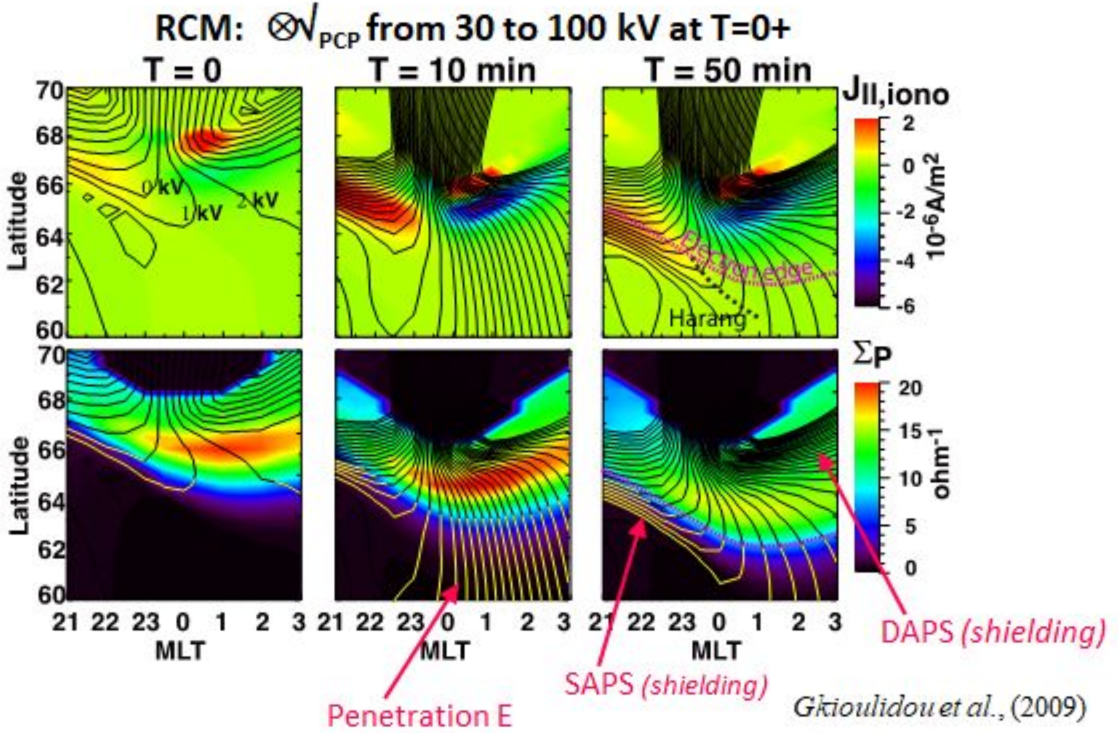

Gkioulidou et al., (2009)

RCM modeling of bubble introduced at tail outer boundary

[*Yang et al*, 2014; Wang et al., 2018]

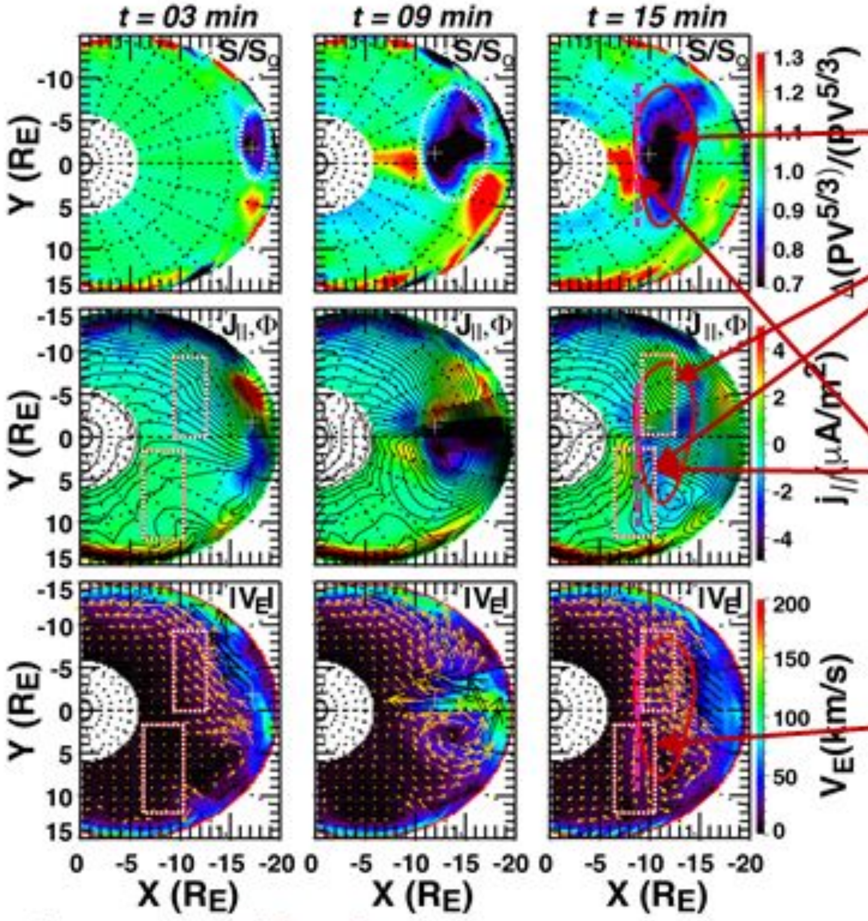

based on *Wang et al.* [2018]

- **B, E drifts spreads bubble** azimuthally near-Earth transition region
- **E and V_E increase with bubble spreading**
  - **Dawnside: within bubble**/R1 (DAPS). *(Liu et al., 2018)*
  - **Duskside: within R2/SAPS** equatorward of bubble *(Makarevich et al., 2011; Lyons et al., 2015; Gallardo-Lacourt et al., 2017)*
- Gives **longitudinally extended upward $j_{||}$**
- **Onset instability via large change in entropy gradient**??
  - Extends E-W due to bubble spread??
- **Can measure flows,** not bubble

Poker FLAT ISR, ASI

Azimuthal diversion of streamer flow

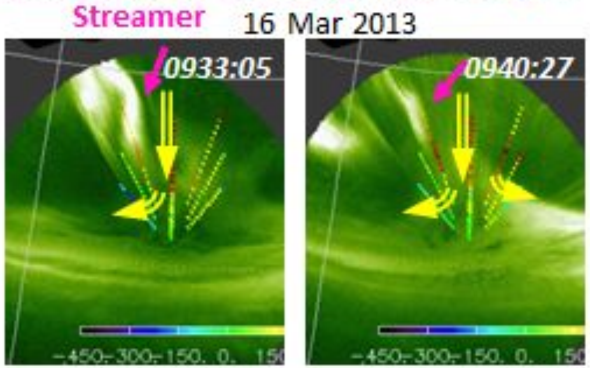

Flow channel directly to onset

21 November, 2012 0803:20 onset

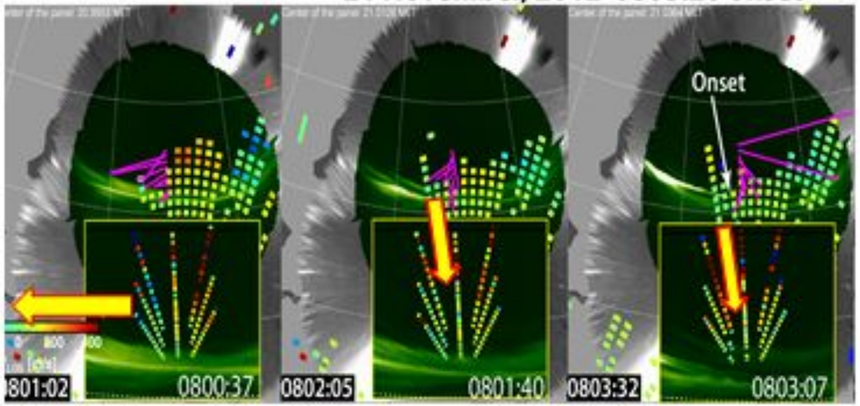

DAPS increase: onset eastward expansion

15 March 2013, 1051:15 UT onset

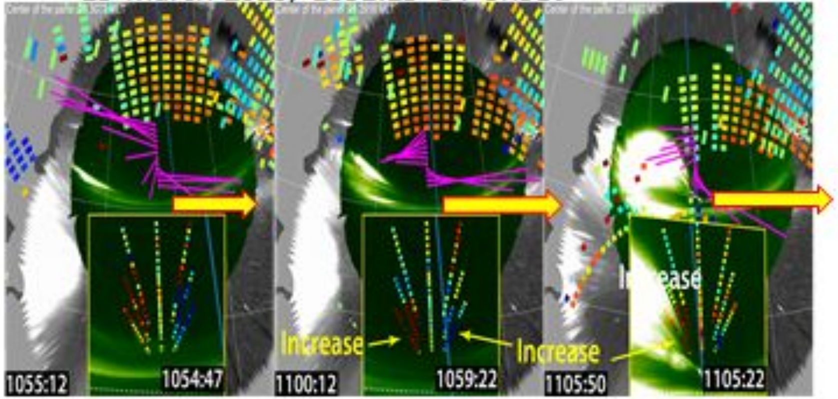

SAPS increase, flow to surge: onset westward expansion

9 March, 2013 0902:55 onset

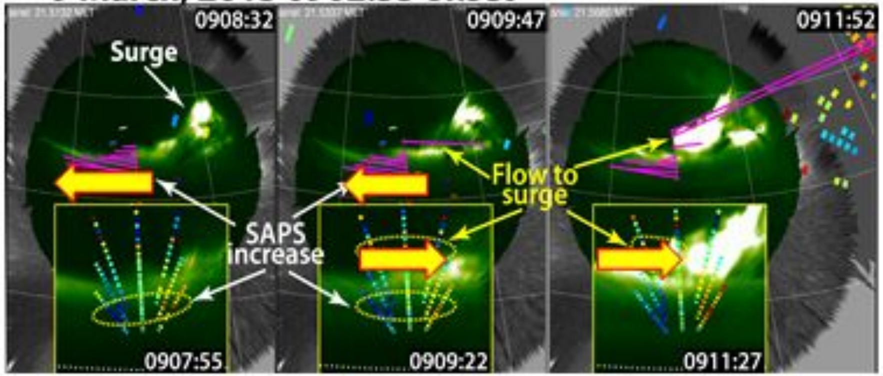

Russell Landry, UNM

Storm-time DMSP Poynting flux measurements and conductance estimations

Russell Landry
Christos Christodoulou
University of New Mexico

- Integrated DMSP measured Poynting flux during 44 geomagnetic storms (2000-2012)
- Used storm main phases with defined Newell boundaries

Integrated Poynting Flux

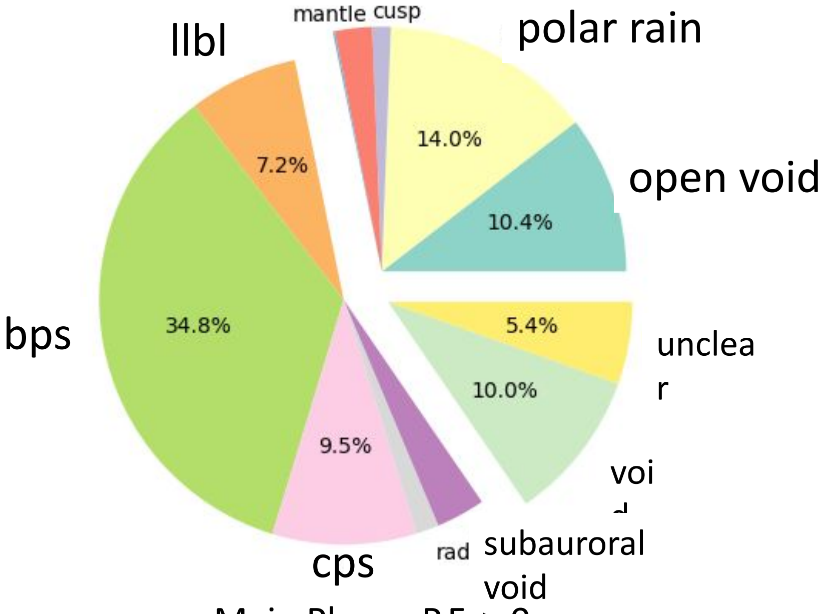

Main Phase, P.F. > 0

- Estimated conductance from particle precipitation spectra
  - Fang et al. (2010) - electron impact ionization rates
  - Fang et al. (2013) - ion impact ionization rates
  - Assume chemical equilibrium, Rees (1989) recomb. coeff.s
  - T_e and NO^+, O_2^+ concentration ratio from IRI
  - T_n and neutral density from MSIS
  - Solar conductance from Moen and Brekke (1993)

Main Phase, Σ_P from Solar EUV + Precip.

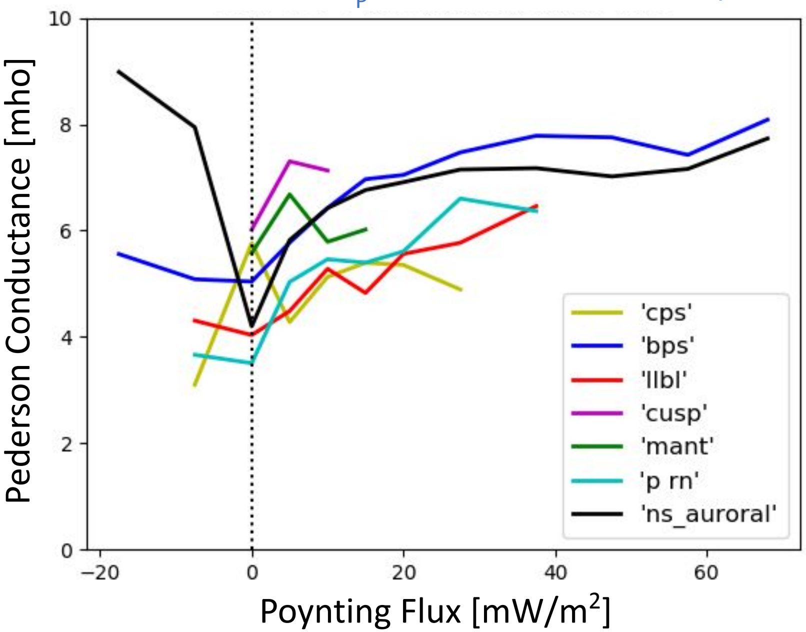

Median Poynting Flux ($\frac{1}{\mu_0}\vec{E}\times\Delta\vec{B}$)

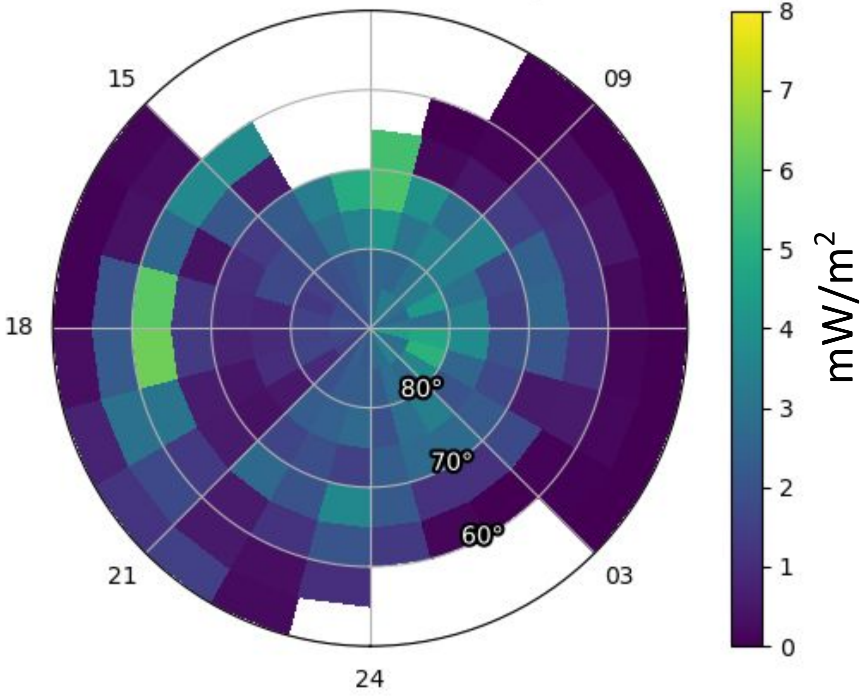

Median Joule Heating ($\Sigma_P E^2$)

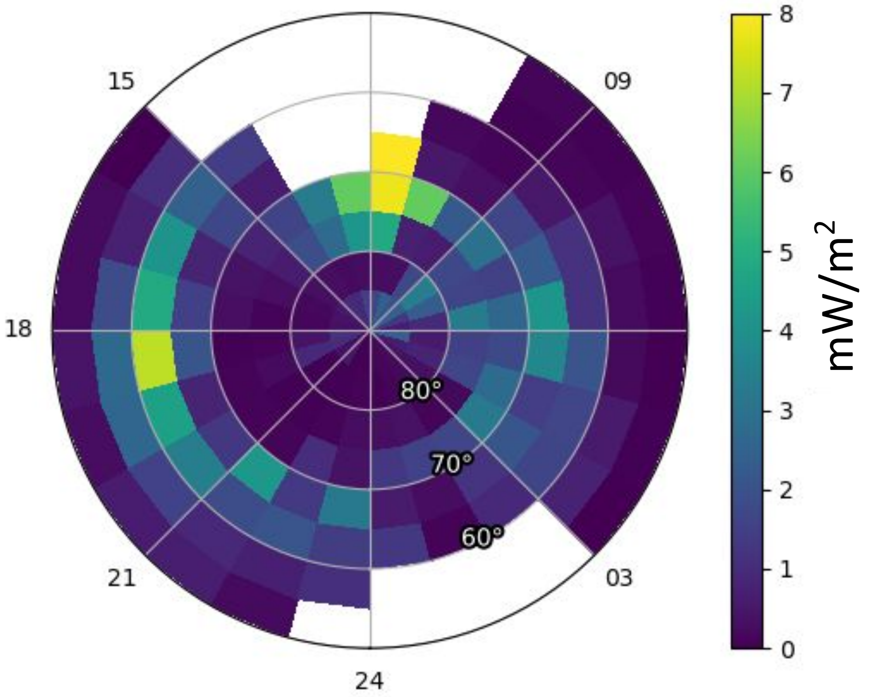

- Main phase
- Southward B_Z
- Both Hemispheres

$$\frac{\text{Integrated P.F.}}{\text{Integrated J.H.}} = 89.4\%$$

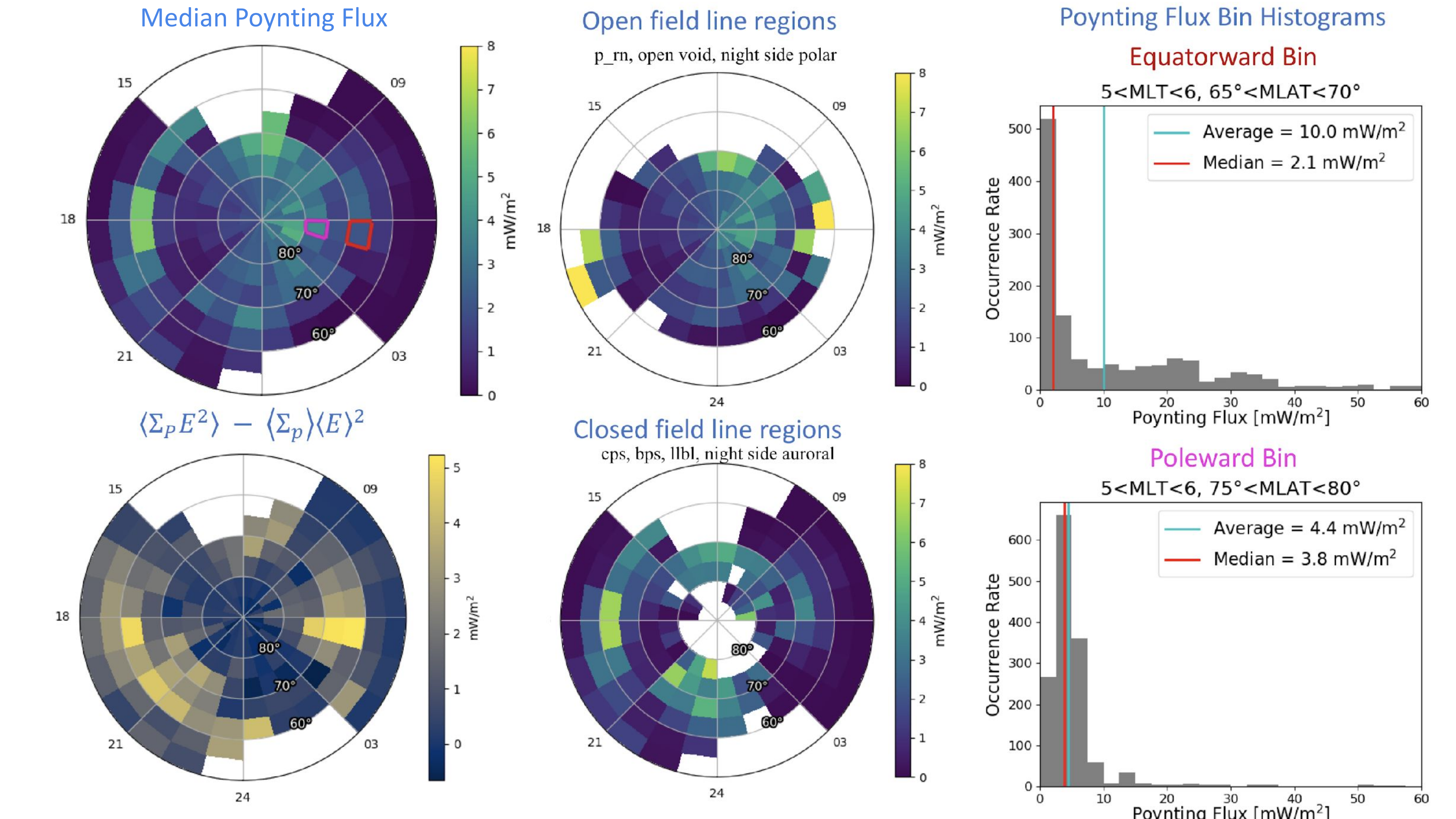

Median Poynting Flux
mW/m^2
Open field line regions
p_rn, open void, night side polar
mW/m^2
Poynting Flux Bin Histograms
Equatorward Bin
5<MLT<6, 65°<MLAT<70°
Average = 10.0 mW/m^2
Median = 2.1 mW/m^2
Occurrence Rate
Poynting Flux [mW/m^2]
$\langle \Sigma_P E^2 \rangle - \langle \Sigma_p \rangle \langle E \rangle^2$
mW/m^2
Closed field line regions
cps, bps, llbl, night side auroral
mW/m^2
Poleward Bin
5<MLT<6, 75°<MLAT<80°
Average = 4.4 mW/m^2
Median = 3.8 mW/m^2
Occurrence Rate
Poynting Flux [mW/m^2]

Michael Negale, SDL

Tracking Polar Cap Patches Using a Reconstructed Ionosphere

M. Negale[1], J. Holmes[2], T. Parris[2], D. Ober[2], E. Dao[2], R. Kelly[1], V. Eccles[1], J. Hines[1], and T. Pedersen[2]
[1] Space Dynamics Laboratory, [2] Air Force Research Laboratory

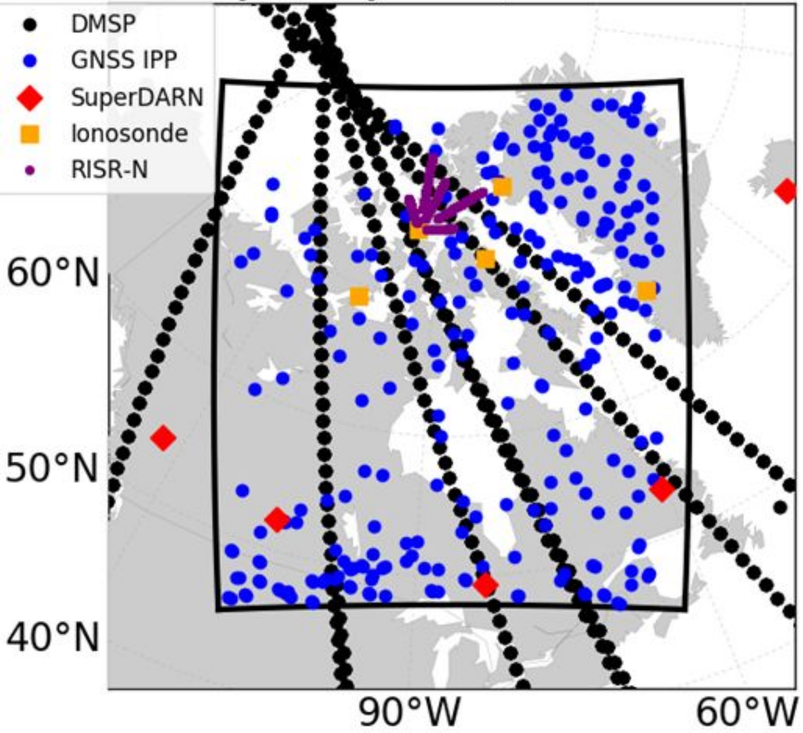

- GPS Ionospheric Inversion (GPSII)
  - North West Research Associates (NWRA)
- Reconstructed the high-latitude ionosphere
  - 22 January 2012 during a moderate geomagnetic storm triggered by a coronal mass ejection.
- Results shown for two GPSII reconstructions:
  - GNSS, Ionosondes, SuperDARN
  - GNSS, Ionosondes, SuperDARN, DMSP, and RISR-N
- Solutions obtained every 5 min from 20 – 24 UT
  - 78 GNSS receivers, 5 Ionosondes, 4 DMSP satellites, and 5 SuperDARN radars.

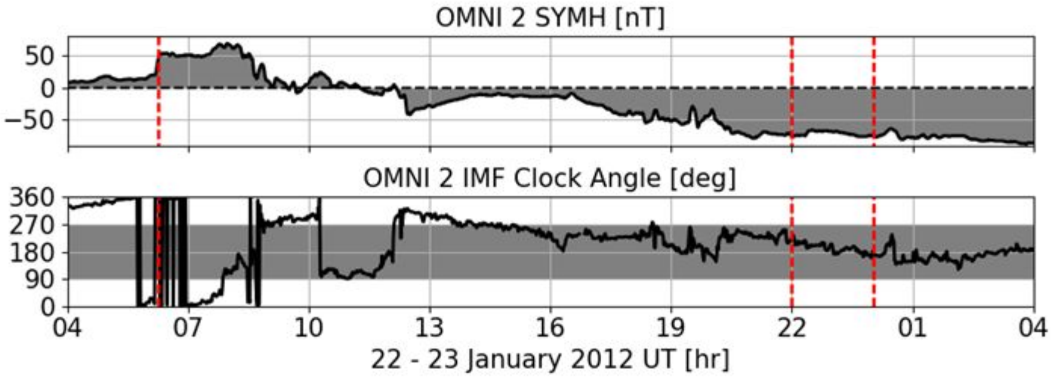

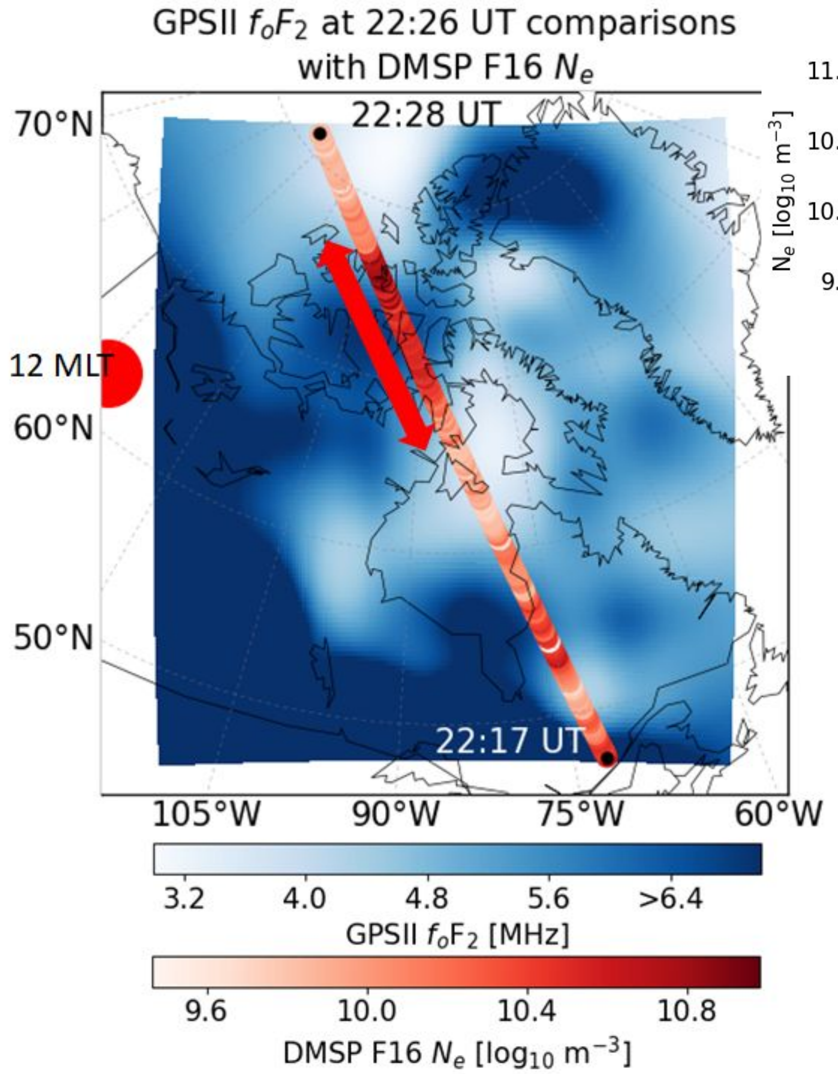

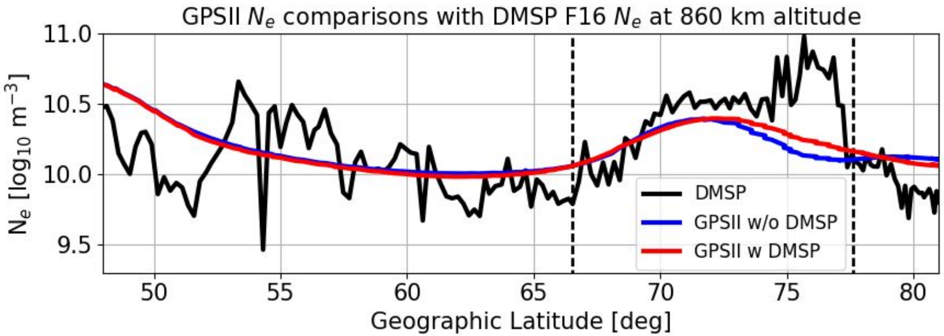

Polar cap patches observed by DMSP satellites and RISR-N were successfully reconstructed by GPSII.

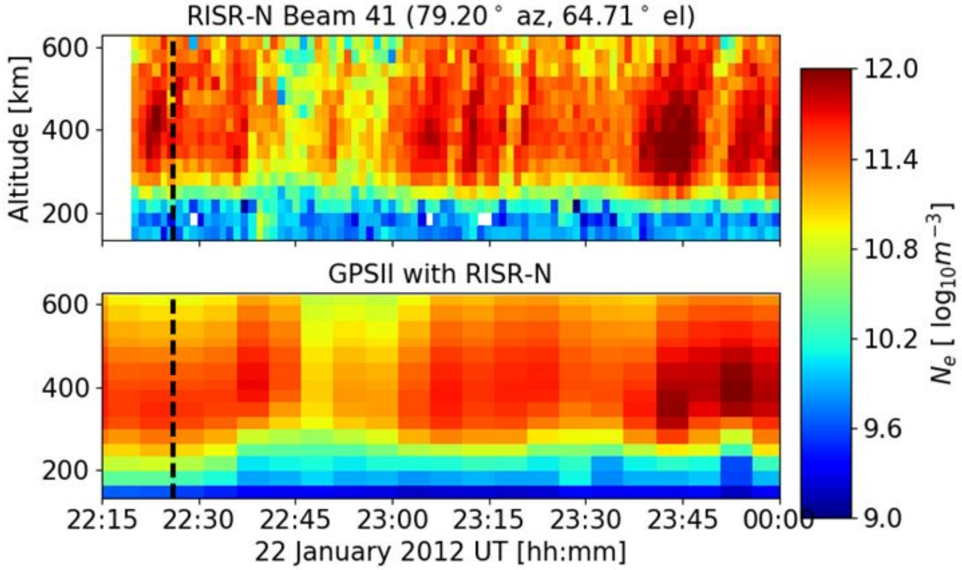

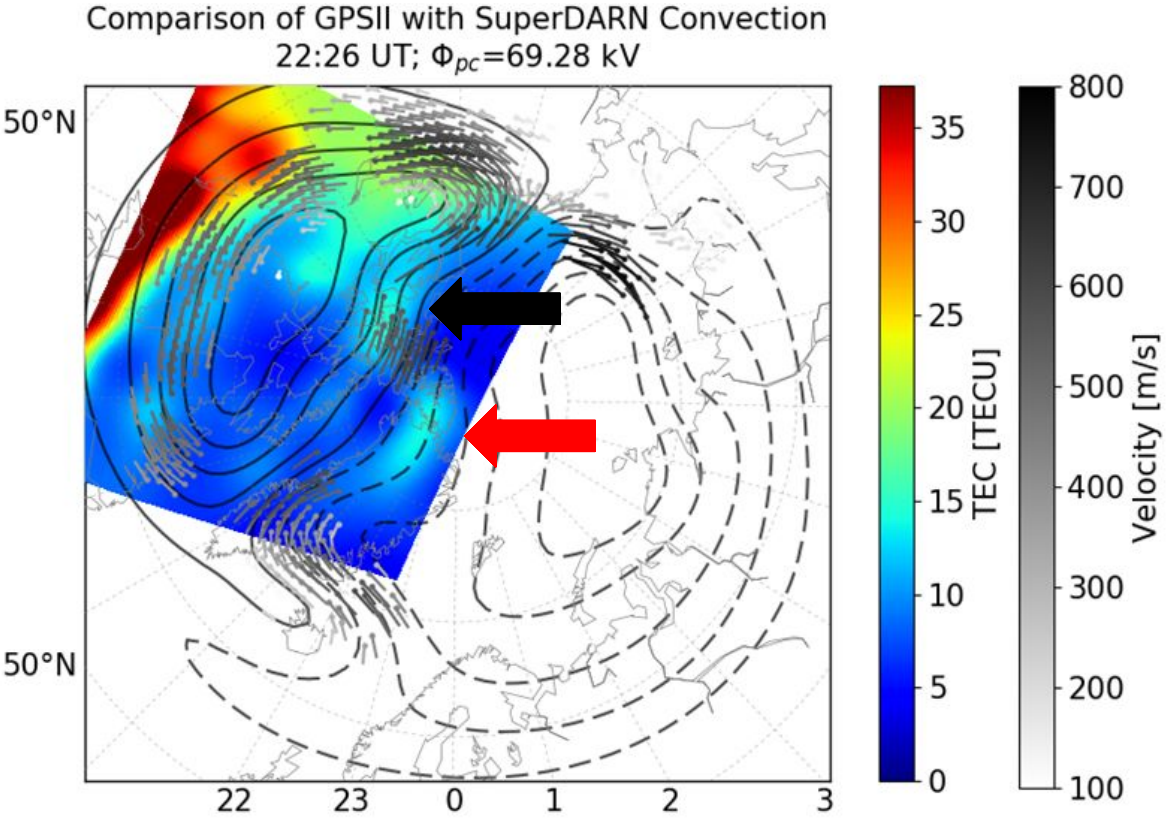

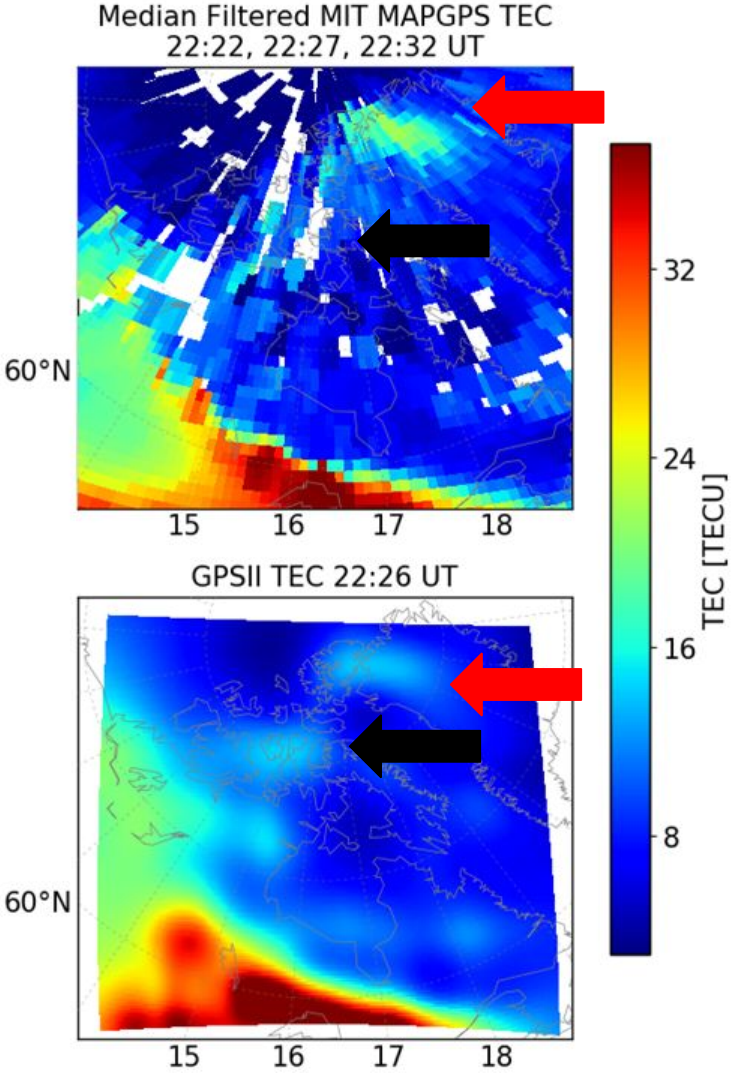

- GPSII reconstructed ionosphere agrees very well with SuperDARN ionospheric observations.
- GPSII capable of reconstructing the complex high latitude ionosphere.

Joaquin Diaz Peña, BU

We can use AMISR capabilities to do a 3D map of the density by interpolation.

- Patches can then be identified and characterized including their altitude structure.
- Approximate velocity of the plasma can also be obtained by this method.
- By Including OMTI images a better understanding of events is acquired.

This particular event had steady Bz positive and By negative and several auroral arcs (red line)

High latitude reconnection should be expected.

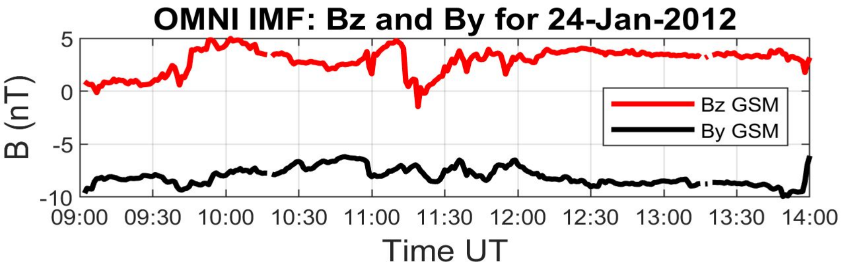

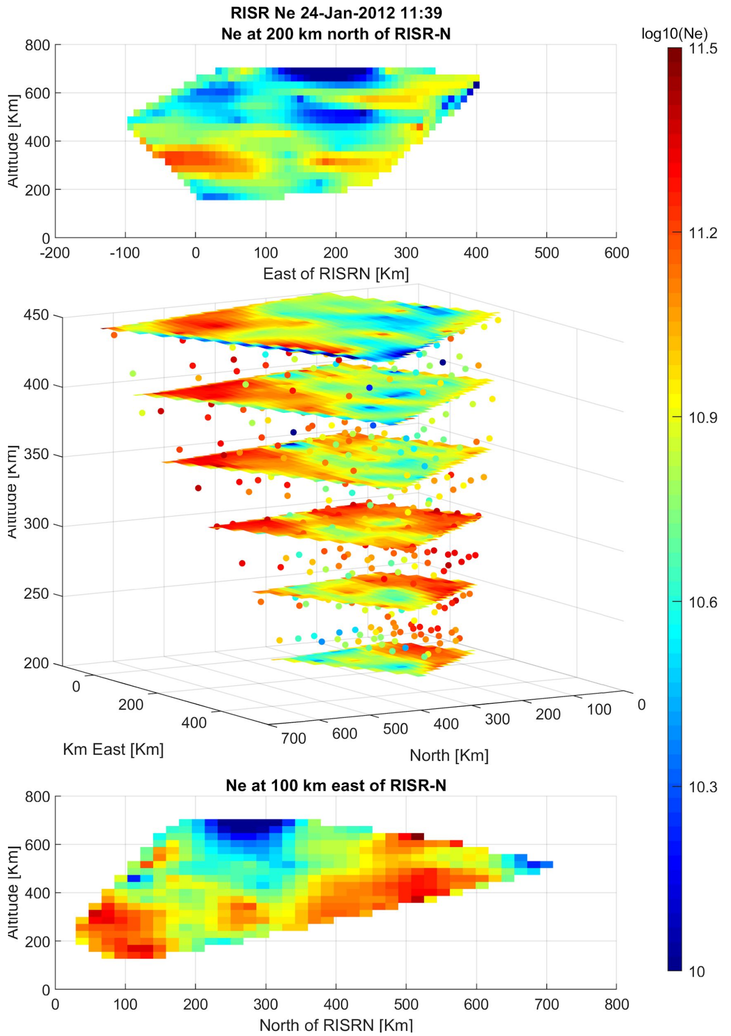

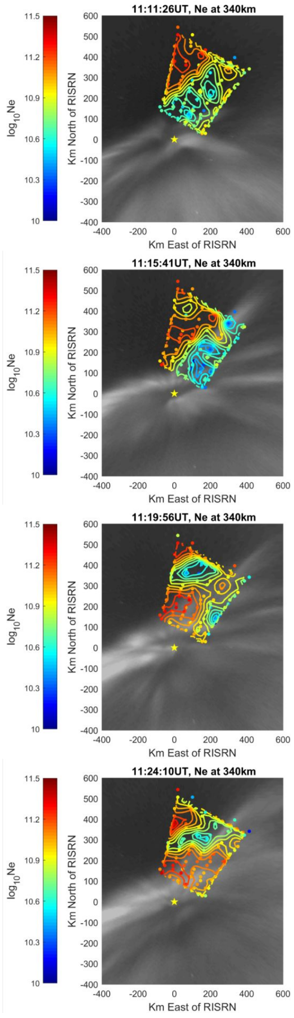

By approximately following the center, and thus moving **in the frame of reference of the F region patch** we can create a time series (going from darker to lighter color in the figure) to study the time evolution of the patch as it moves towards the OCB.

- Maximum density remains steady through time
- Both temperature and pedersen conductivity remain steady in time **until the patch touches the auroral arc.**
- At this time there is an enhancement in temperature and low altitude density.

The sudden low altitude density enhancement occurs in a time interval of less than 4 minutes. **This affects the lower altitude pedersen conductivity.**

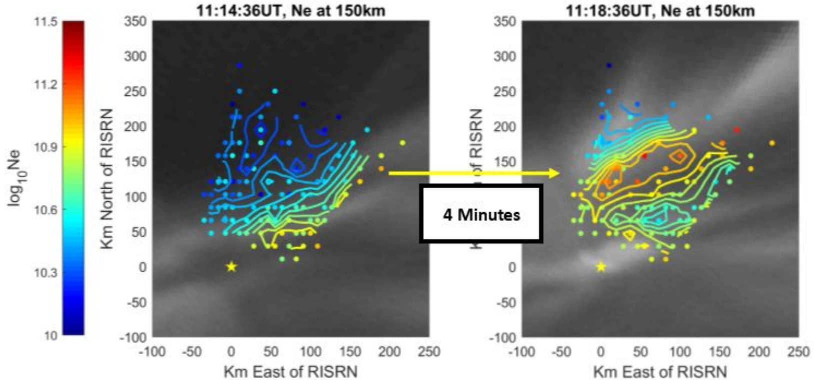

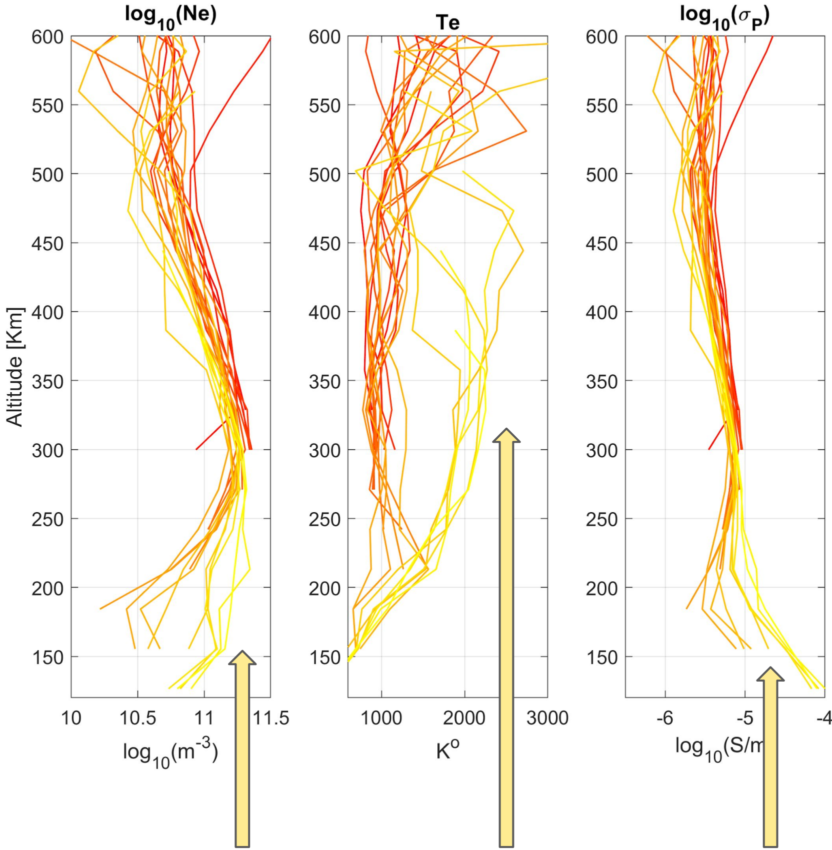

F region patch touches aurora

We can estimate the **height integrated Pedersen**.

- Conductivity is a constant 2 S above 180 Km.
- Below 180 Km it is shown to spike when touching the arc, surpassing the values above and thus dominating the total value

By assuming a neutral wind at rest, it is possible to compute an approximate Joule heating rate in the frame of reference of the patch.

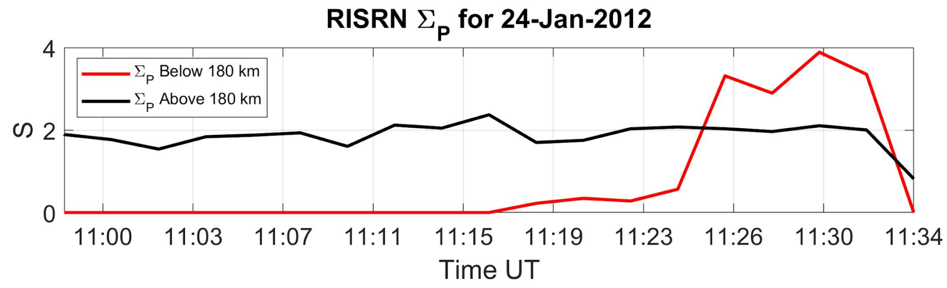

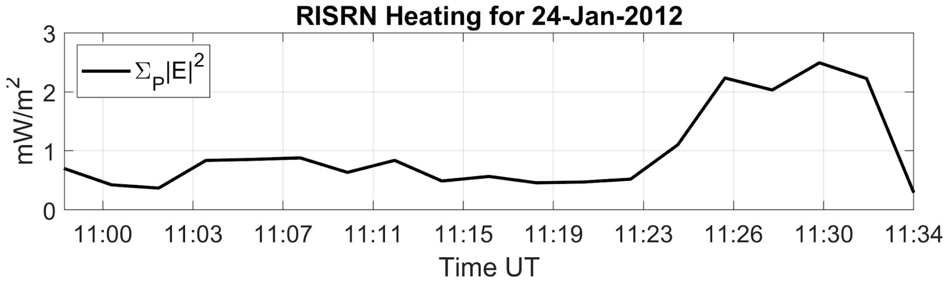

A pass from DMSP F16 happened at the same time going over RISRN, and energy deposition is calculated on its orbit It shows the highest energy inside the auroral arc at 4mW/m2.

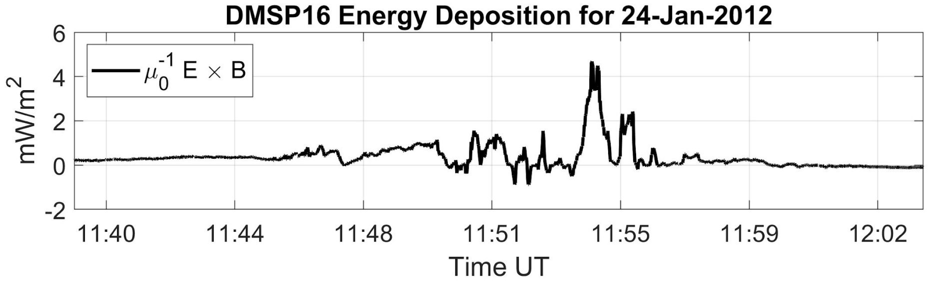

Conclusion:

- σp enhancements leads to an large local Joule heating at the peak of the F region and below.
- AMISR has great capabilities to study the small scale dynamics of the polar cap.
- There is a need to use both modeling and observations to discern between if the movements are due to diffusion, transmort, convection, etc.

Zihan Wang, UM

Segmentation of SED by Boundary Flows Associated with Westward Drifting Partial Ring current (Sep 7, 2017 storm)

Simulation results from GITM driven by coupled BATSRUS and RCM

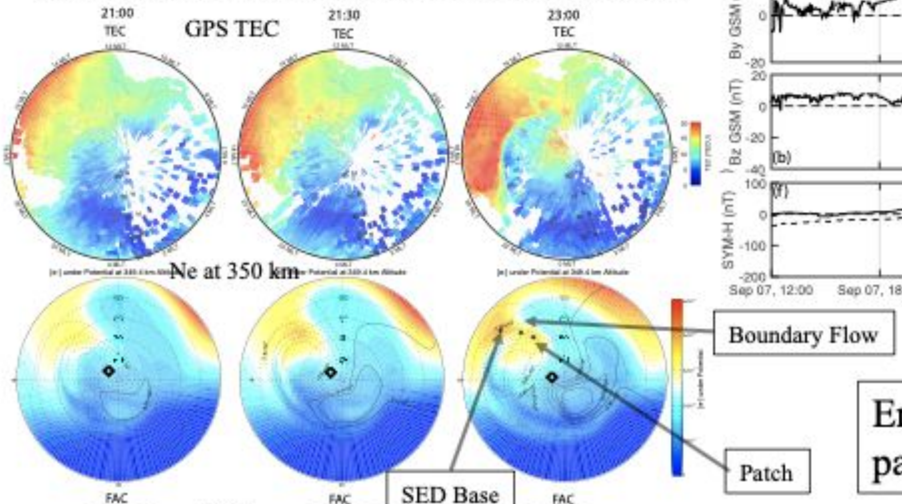

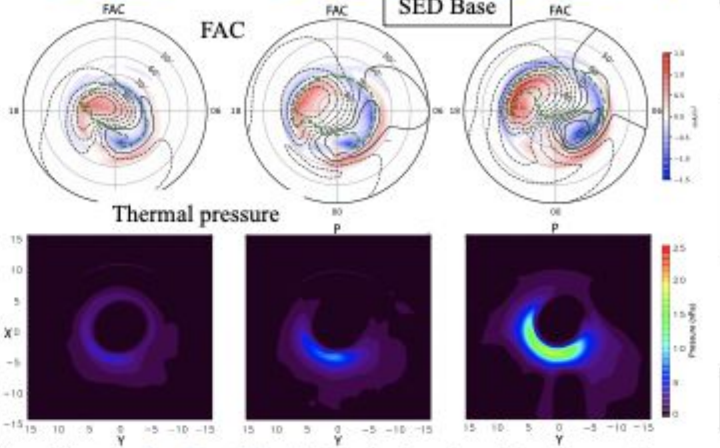

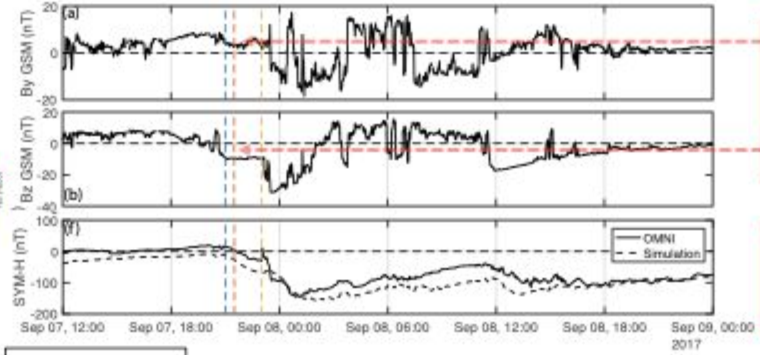

Almost constant IMF By and Bz when segmentation occurred.

No FTE in the simulation results.

Enhanced boundary flows segmented SED plume into patches at 2300 UT.

Region 2 FACs near 15 MLT enhanced corresponding to the west drifted partial ring currents. Closure of region 1 and 2 FACs led to large boundary flow.

Partial ring currents drifted westward when the storm developed.

Zihan Wang (wzihan@umich.edu), Shasha Zou, Jiaen Ren, Thomas Coppeans, Aaron Ridley, Tamas Gombosi

Field line tracing to the magnetosphere

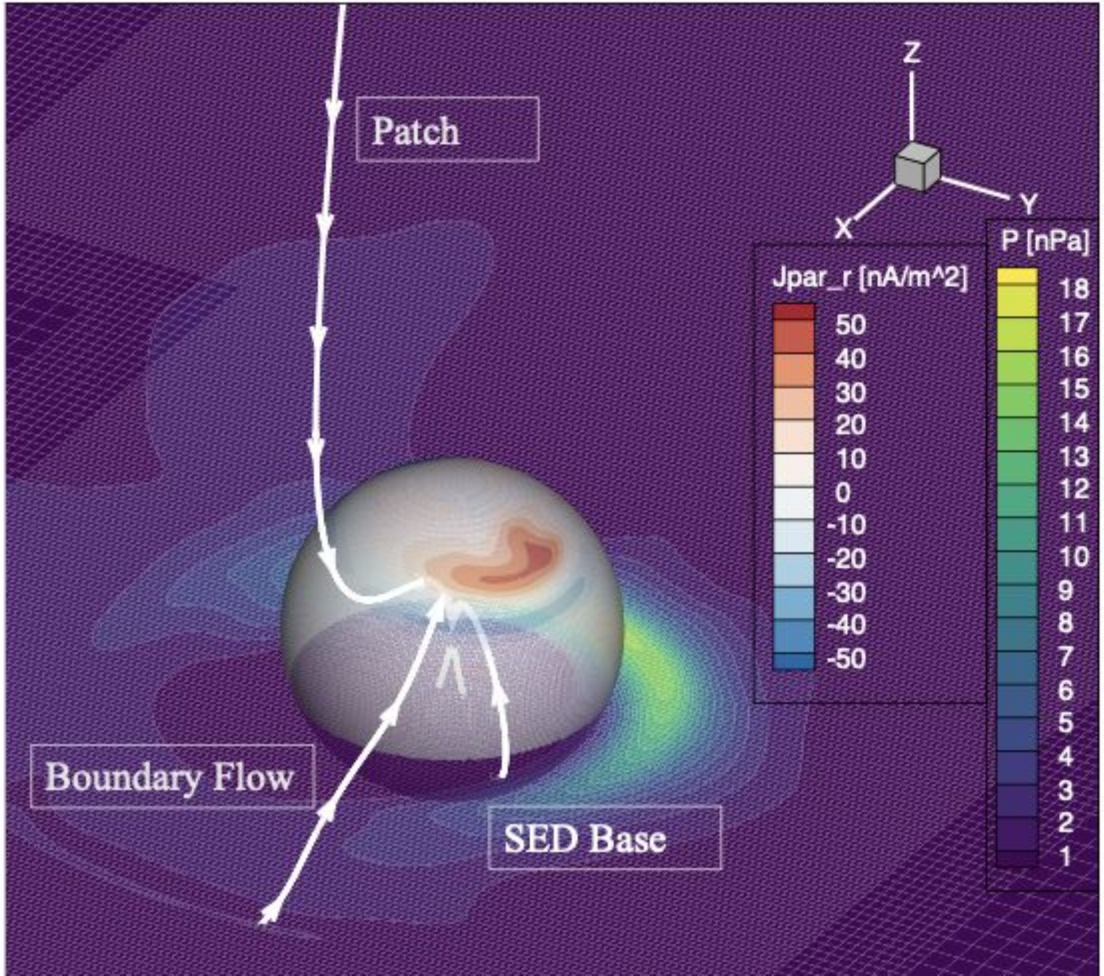

Polar cap patch: On open magnetic field lines and connected to the solar wind.

SED base: On the inner edge of the partial ring current.

The boundary flow region: Mapped to the outer boundary of the partial ring current (poleward boundary of Region 2 FACs in the ionosphere). This proves that the segmentation was due to the boundary flows located between the Region 1 and Region 2 FACs.

How the boundary flow segments the SED plume?
Transportation or local loss?

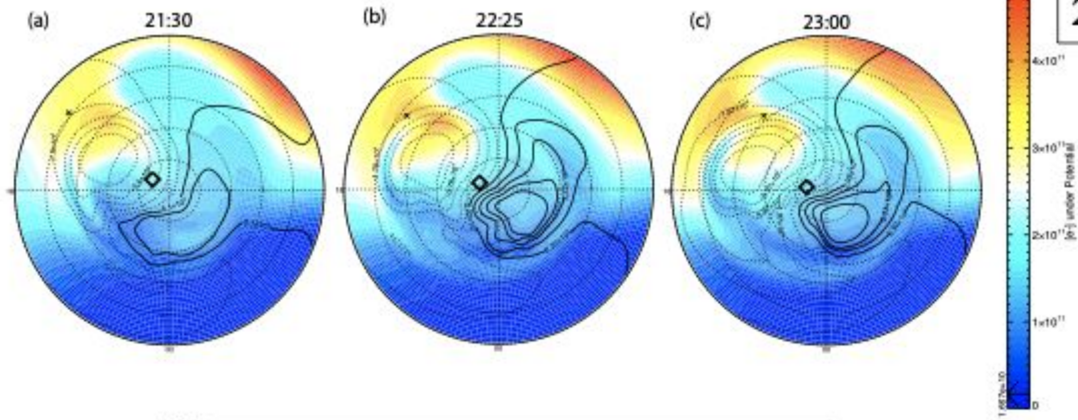

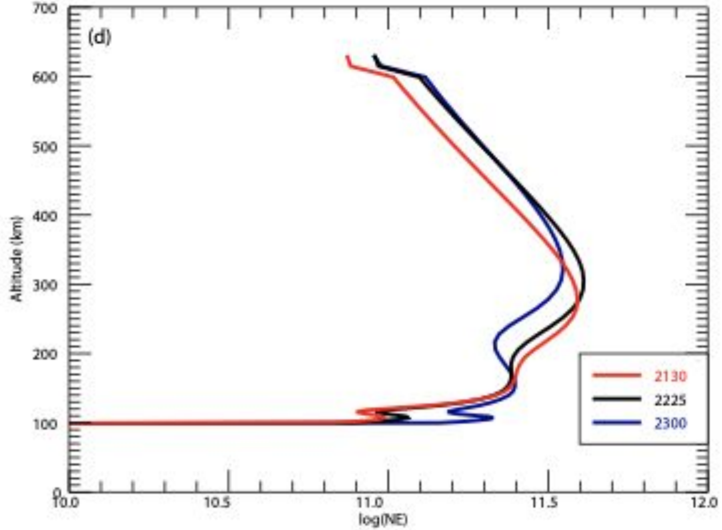

The plasma parcel at the center of the boundary flow at 2300 UT was traced backward in time to 2130 UT to identify its source region.

Two different phases: Growing phase between 2130 and 2225 UT, decaying phase between 2225 and 2300 UT.

Growing phase: Plasma was lifted to higher altitudes. Projection of the northward convection flows in the vertical direction.

Decaying phase: Enhanced frictional heating due to boundary flow led to the electron density decrease in the whole F layer.

Conclusion

- **Enhanced boundary flows between Region-1 and Region-2 FACs segment SED plume into patches.**
- **Localized plasma loss due to enhanced frictional heating within boundary flows.**
- **During this process, no IMF variations or transient reconnections are required.**

Ying Zou

Effects of Substorms on High-Latitude Upper Thermospheric Winds

Ying Zou (BU/UCAR), Y. Nishimura, L. R. Lyons, M. Conde, R. H. Varney, V. Angelopoulos, S. Mende

Ground-based FPI measurements

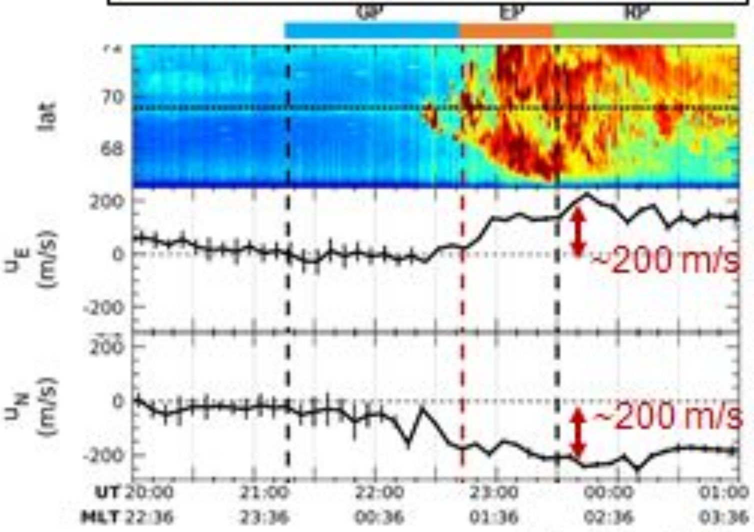

Cai et al., 2019

Superposed CHAMP measurements

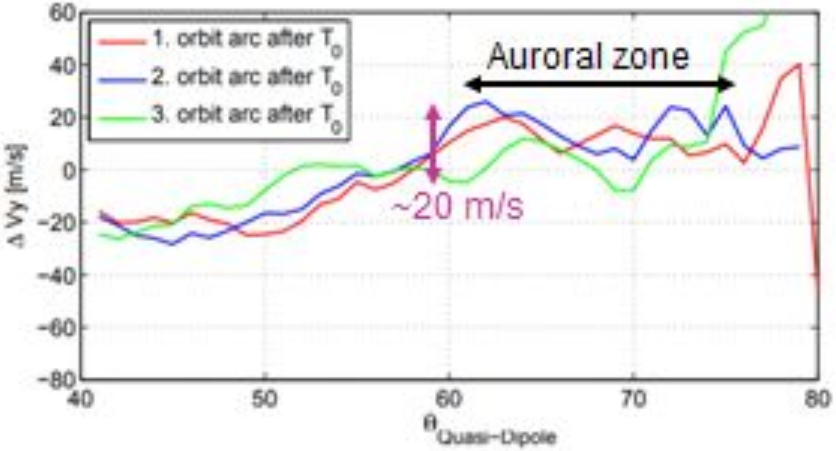

Ritter et al., 2010

Significant change (~200 m/s) ? ***Insignificant change (~20 m/s)***

Motivation: obtain 2D synoptic map of thermospheric wind perturbations of substorms.

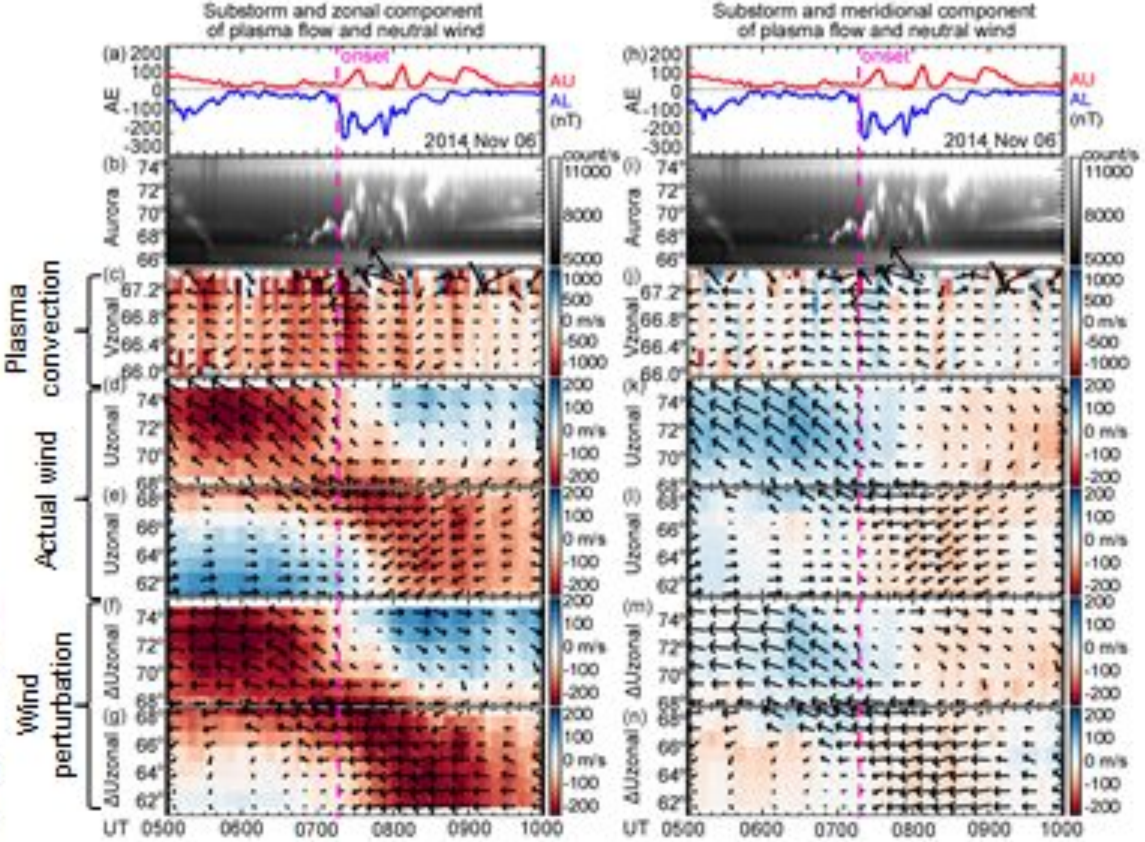

One observational example

- Before onset, winds are westward.
- Following onset, winds are accelerated east- and westward at and equatorward of the auroras, respectively.
- The accelerated winds are 100-200 m/s from pre-substorm quiet time condition.

Effects of substorms on the thermosphere

ΔU before substorm onset **ΔU after substorm onset**

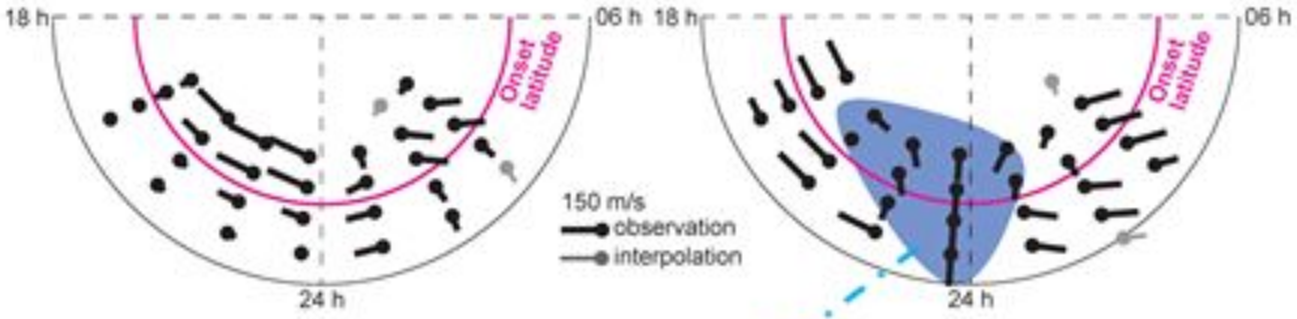

In comparison with effects of substorms on the ionosphere

Plasma convection after onset

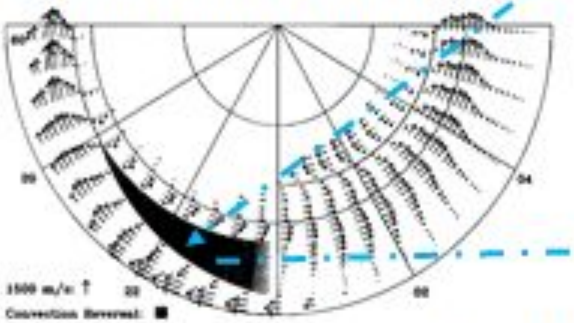

Substorm electrojet system

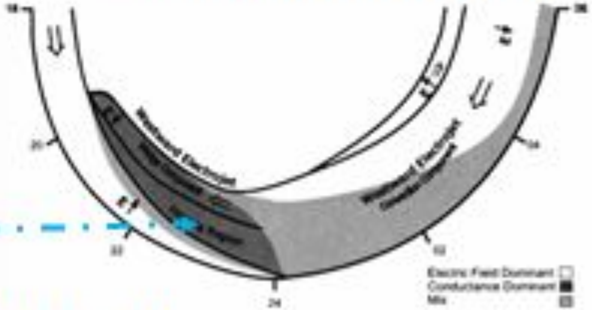

Gjerloev and Hoffman, 2001

Olga Verkhoglyadova, JPL

Importance of Magnetosphere-Ionosphere-Thermosphere coupling at meso- and small-scales

O. P. Verkhoglyadova, X. Meng, D. Ozturk[1], J. Semeter[2], R. Varney[3], A. Reimer[3] and S. Kaeppler

[1]Jet Propulsion Laboratory, California Institute of Technology, Pasadena, CA;
[2] Boston University, Boston, MA; [3] SRI International, Menlo Park, CA; [4] Clemson University, Clemson, SC

IT deposition → $\vec{j} \cdot \vec{E} + \nabla(\vec{S}) = 0$ ← Magnetospheric source

$$\vec{S} = \frac{1}{\mu_0}[\vec{E} \times \vec{B}]$$

- Coupling, energy transport in the geospace environment and e/m energy deposition in the ionosphere-thermosphere (IT) depends on temporal and spatial scales (Huang and Burke, 2004; Semeter et al., 2010; Lyons et al., 2016; Huang et al., 2016; McGranaghan et al., 2017+)

- Physical mechanisms and efficiency of the magnetosphere-IT coupling also differ depending on their scale.

- Ignoring meso- and small-scale processes can lead to under-estimation of IT energy budget

How do we estimate JH from observations?

Across different spatial scales, there are different approaches for Joule heating estimates using satellite, rocket and ground-based measurements.

- Incoherent Scatter Radar (*e.g., Thayer, 1998; Fujii et al., 1998; Fujii et al., 1999; Thayer, 2000, Cosgrove et al., 2009*)
- Satellite-based: *The Assimilative Mapping of Ionospheric Electrodynamics (AMIE) procedure* (e.g., *Lu et al., 1995; Chun et al., 1999; Knipp et al., 2004; McHarg et al., 2005)*
- Rocket-based (e.g., *Evans et al., 1977; Sangalli et al., 2009; Hurd et al., 2016*)

$$\sigma_p E^2$$

$$\vec{j} \cdot \vec{E} = \vec{j} \cdot \vec{E}' + \vec{V}_n \cdot \vec{j} \times \vec{B} \qquad \vec{V} = \sum_\alpha \frac{n_\alpha m_\alpha \langle \vec{V}_\alpha \rangle}{n_\alpha m_\alpha}$$

Joule heating at mesoscale

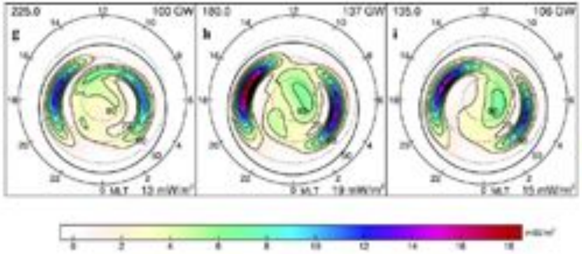

Empirical model at 110 km altitude
(*Weimer, JGR, 2005*)

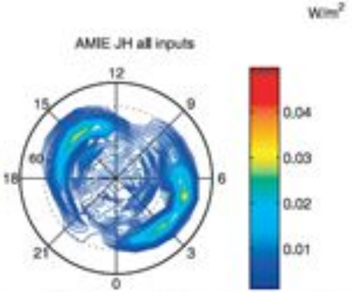

AMIE reconstruction of Joule heating for 11:10 UT on 15 May 1997 (*McHarg et al., 2005*)

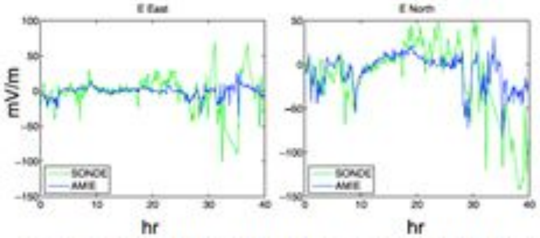

Eastward and northward E components measured by Sondrestrom (green) and modeled by AMIE (blue) starting 9 Jan 1997 (*Cosgrove et al., 2009*)

✓ ***JH estimation depends on spatial and temporal resolutions of the method***

Energy transfer rate is scale-dependent (*Thayer and Semeter, 2004*) and resolution-dependent (*Deng and Ridley, 2007; Deng et al., 2009; Cosgrove et al., 2009, 2011*)

Dogacan Ozturk, JPL

Modeling meso-scale electric field variability through GCMs

Dogacan S. Ozturk[1], Xing Meng[1], Olga Verkhoglyadova[1], Josh Semeter[2], Roger Varney[3], Ashton Reimer[3]

1: Jet Propulsion Laboratory, California Institute of Technology; 2: Department of Electrical and Computer Engineering and Center for Space Physics; Boston University; 3: Stanford Research Institute

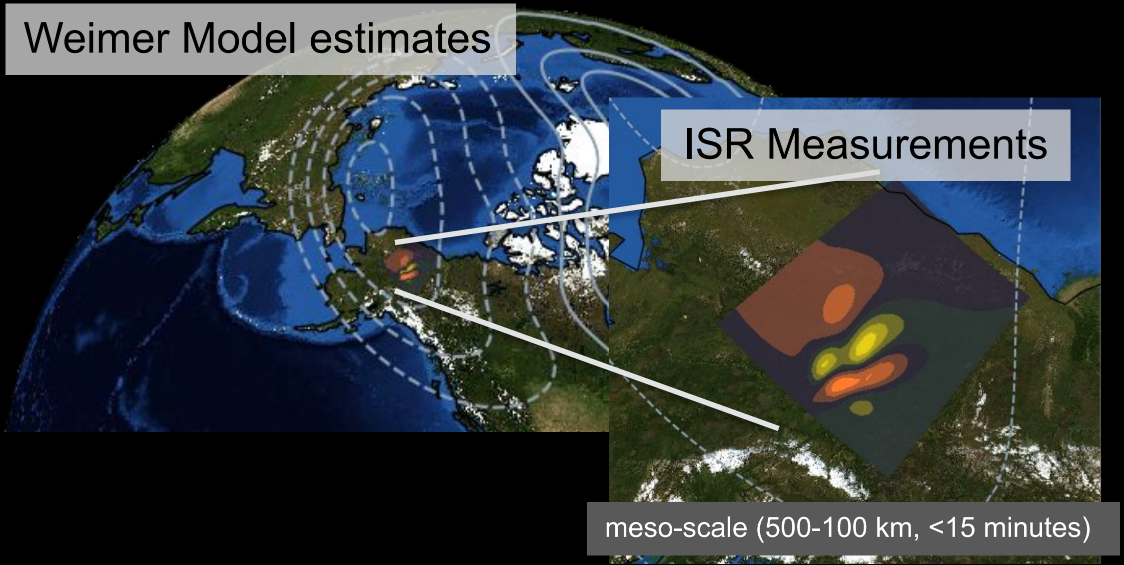

- Global Circulation Models (GCMs) traditionally use empirical models for global estimates of **electric fields and conductivity** and significant work is ongoing to resolve meso-scale structures[1].
- Missing meso-scale electric field variability (temporal + spatial) causes **underestimation of energy input and dissipation in the high-latitude Ionosphere**[2].

1 Codrescu et al. 1995; Deng et al. (2009); Cousins et al. (2013)
2 Cosgrove et al. (2009); Huang et al. (2014); Brinkman et al. (2016)

Our aim is to understand **the role of meso-scale electric fields in energy dissipation at high-latitude I-T system**. This talk summarizes our efforts in quantifying dynamic driving using ISR measurements and adapting a first-principles model to dynamical driving.

Jet Propulsion Laboratory
California Institute of Technology

contact: dogacan.s.ozturk@jpl.nasa.gov

PFISR LOS velocity measurements can be used to derive Electric fields on a 2D grid*.

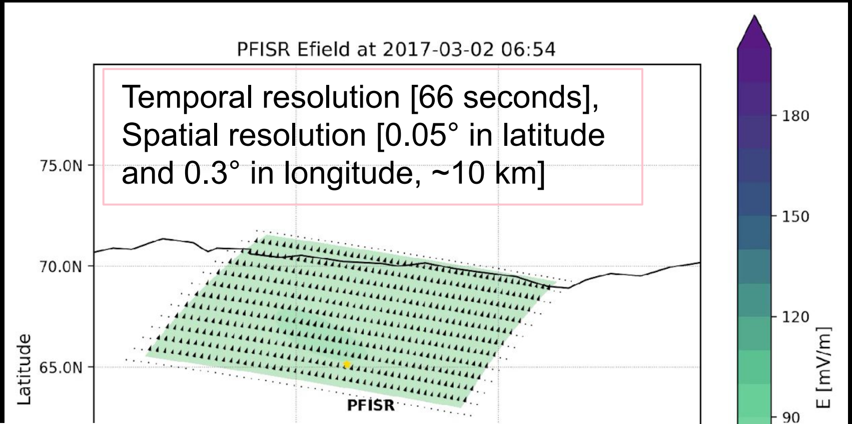

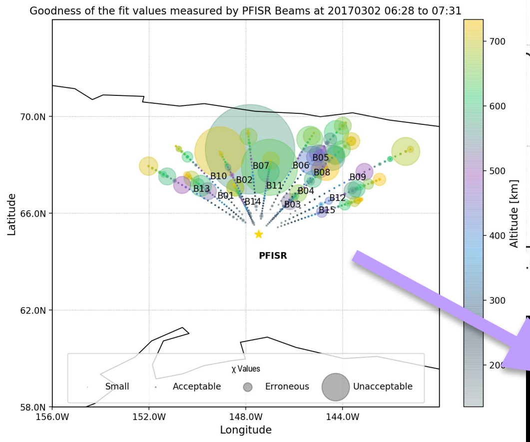

PFISR aiding the ISINGLASS experiment with 15 beams operating [Clayton et al., 2019, JGR]

→Calculate and subtract 30 min. average from measurements

E_total=E_background+E_variability

→Down sample and calculate the potential differences in new grid (0.75°x0.75°)

→Merge the calculated potentials with Weimer potentials to obtain a global potential pattern

→Drive **GITM1** with the new potential patterns

→Validate results with comparisons of PFISR Ne, Te, and Ti measurements along the beams

- Certain beams are more reliable
- Errors guide validation efforts

* Procedure requires certain amount of beams, data courtesy of Roger Varney and Ashton Reimer.

[1] Ridley, Deng and Toth, JASTP, 2006

Plasma profiles vary for different drivers.

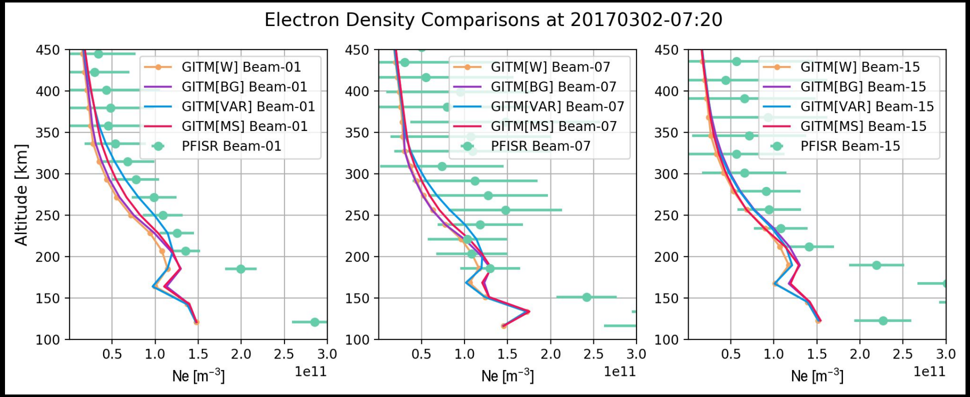

Variability seems to play an important role in electron density above 150 km.

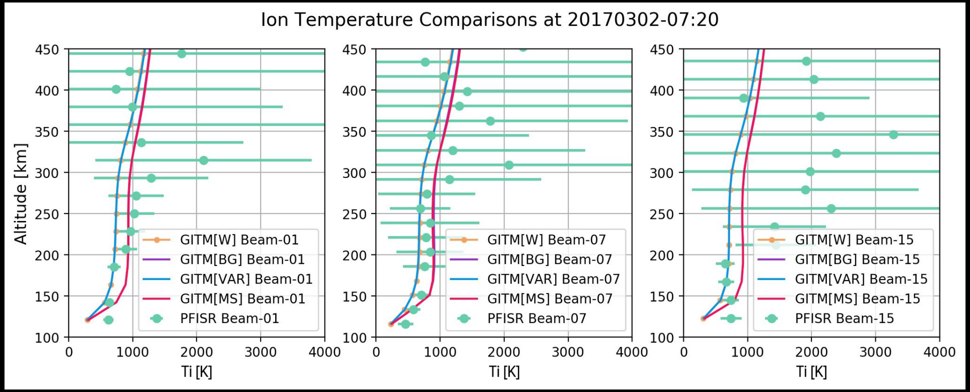

Ion temperature estimates are improved above 200 km, once the background and total electric fields are employed.

Key Points

- We are developing a framework that can utilize **any local (meso-scale) 2D electric field measurement** as input to run a global I-T model.
- Different drivers performed better depending on time and altitude.
- Electron density significantly underestimated below 200 km.

Future work

- Investigate the effects of meso-scale electric fields on the **global energy budget** during active geomagnetic periods.
- Validation Studies: More events, more conjunctions, different sets of measurements
- Error and uncertainty quantification in measurement input and modeling results

Qingyu Zhu, UTA

Impact of the binning methods on the high-latitude electrodynamic forcing: static vs boundary-oriented binning methods

Qingyu Zhu, Yue Deng, Arthur Richmond, Astrid Maute, Rod Heelis, Marc Hairston, Yun-Ju Chen,
Liam Kilcommons, Delores Knipp, Robert Redmon, Elizabeth Mitchell

2019 CEDAR, Santa Fe

Introduction & Motivations

- **Empirical models of the high-latitude electrodynamic forcing are important for general circulation models (GCMs):**
  - Empirical model ← data are typically binned according to their MLATs and MLTs **(Static binning)**
    ➡ Physically smeared ➡ Joule heating underestimation
  - Alternatively, data can be organized according to boundaries **(Boundary-oriented binning)**
    - ➡ Convection reversal boundaries **(CRBs) → Electric potential**
    - ➡ Auroral boundaries **(ABs) → Particle precipitation**

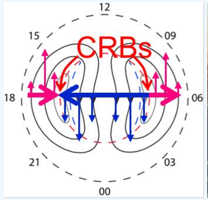

[Chen et al., 2016]

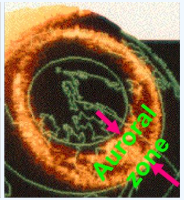

[Credit to NASA]

- **Motivations:**
  - How are boundary-oriented binning results different from the static binning results?
  - How much can Joule heating estimation be affected if high-latitude electrodynamic forcing patterns from different binning methods are utilized to drive a GCM?

Data and Model

DMSP

F16~F18, 2010~2014

Electric potential
→ Cross-track ion drift (SSIES)

Electron precipitation
(SSJ)

Static Binning

Boundary-oriented Binning

GITM

[Ridley et al., 2006]

6 Neutral & 5 Ion Species

Flexible grid resolution

Can provide non-hydrostatic solution

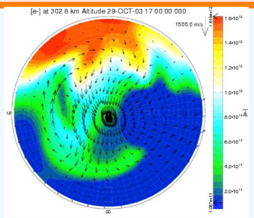

Conditions

All seasons
Both hemispheres

Moderate IMF BZSD

Clock angle: 135°-225°;
Bt: 3~10 nT;

UNIVERSITY OF TEXAS ARLINGTON

Auroral boundaries and CRBs

ABs: Kilcommons et al., [2017]

CRBs: Chen et al., [2015]

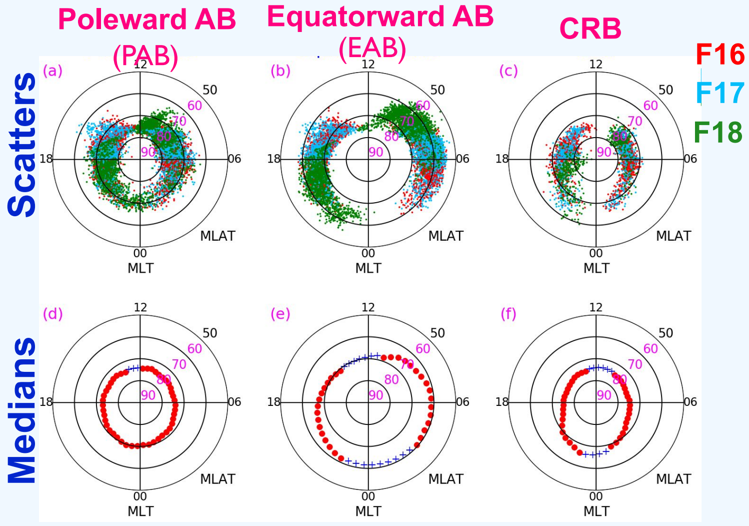

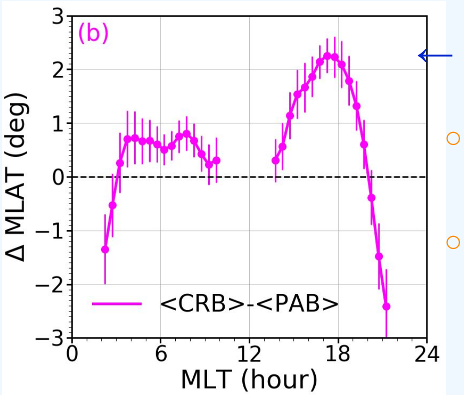

← $MLAT_{CRB} - MLAT_{PAB}$

- CRB is poleward of PAB in general;
- Good alignment between CRB and PAB (Offsets are generally <2°).

Binning results: Static (Top) vs boundary-oriented (Bottom)

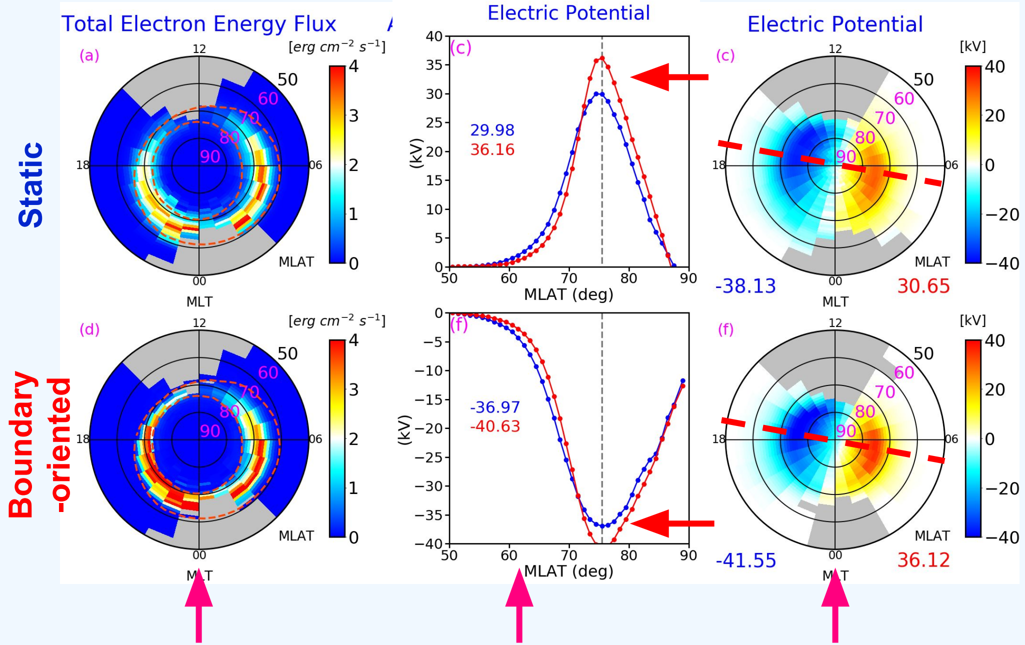

As compared with static binning results, boundary-oriented binning can:

- **Generate** a narrower but more intense electron precipitation pattern
- **Increase** cross-polar-cap potential (CPCP, ~12%)
- **Increase** the electric field magnitude near the CRB

Impacts on Joule heating by using different binning results

(a) Run1 JH: Static pattern (b) Run2 JH: BO pattern (c) (Run2-Run1)/Run1

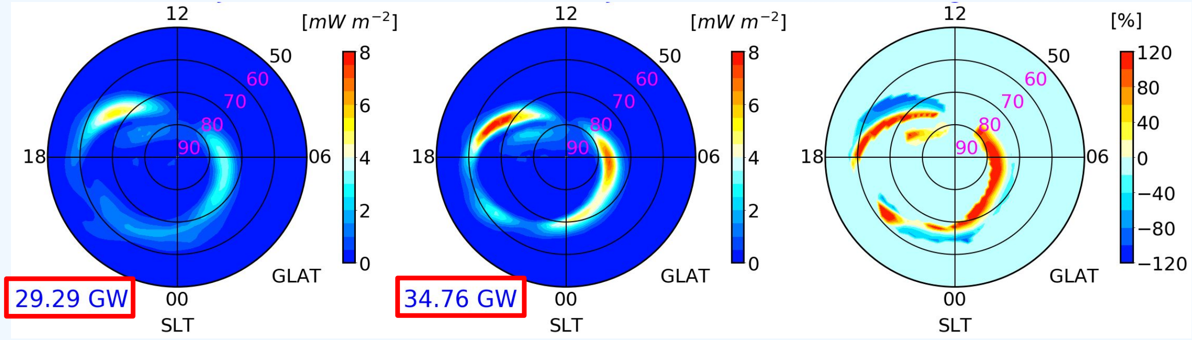

Simulations
- **Run 1: GITM + static binning results**
- **Run 2: GITM + boundary-oriented (BO) results**

- **As compared with Run 1, in Run 2:**
  - Peak values of the Joule heating increase on both dawn and dusk sides;
  - Hemispheric-integrated Joule heating increases by 18% even regions with intense Joule heating are more poleward;

Summary:

For moderate IMF BZSD cases:

- As compared with static binning method, BO method can:
  - **Generate** a more confined and intense electron precipitation pattern;
  - **Increase** the CPCP by 12%;
  - **Increase** the electric field magnitude near the CRB;
- As compared with the simulation driven by static results:
  - Joule heating **increases** by 18% if BO binning results are utilized to drive a GCM.

Thank you!

Ildiko Horvath, UQ

Dayside reconnection and energy deposition observed by CHAMP and DMSP-F13 and modelled by OpenGGCM

Ildiko Horvath and Brian Lovell; The University of Queensland, Australia

31 August 2005 geomagnetic storm (SYM-H_{min} ≈ -120 nT):
A series of neutral density (D_N) enhancements developed in the northern polar region under various IMF conditions.

Correlated CHAMP and DMSP-F13 Scenarios:

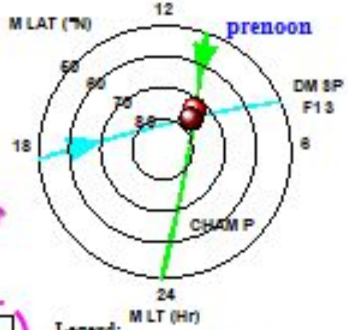

Legend:
E-FC = eastward flow channel
● = E-FC detected by CHAMP at 2252 UT & 0939 MLT
● = E-FC detected by DMSP-F13 at 2339 UT & 0914 MLT

31 August 2005: 1400-2400 UT

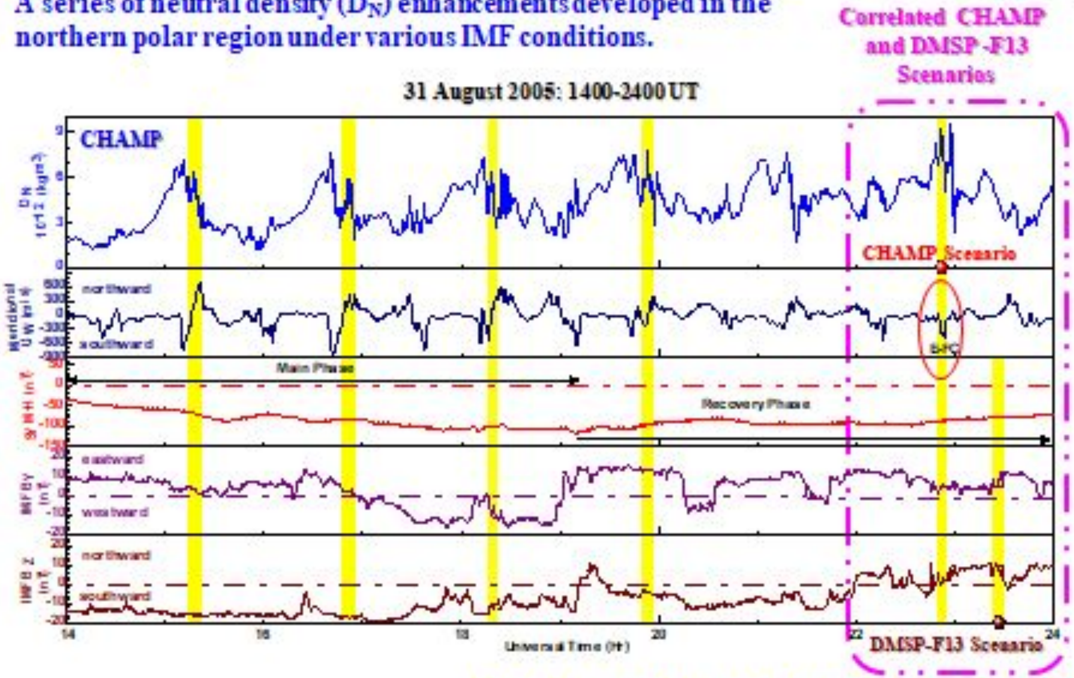

CHAMP Scenario:
A localized polar dayside neutral density enhancement developed within an eastward flow channel (E-FC) of which signature can be seen in the southward meridional wind data.

In both scenarios: $B_Y>0$ → prenoon reconnection
$B_Z>0$ → reverse polar convection

THE UNIVERSITY OF QUEENSLAND AUSTRALIA

CHAMP (at 2252 UT) and DMSP-F13 (at 2339 UT) did not detect the same E-FC because of the 0047 UT difference. But as the underlying IMF conditions were similar, the E-FCs detected were quite similar.

DMSP-F13 Scenario: an eastward flow channel (E-FC) developed at the prenoon particle precipitation zone's poleward edge. Within this E-FC:

- the upward drift (V_{VER}) locally enhanced to ~500 m/s,
- the R1-R2 FACs connected via equatorward Pedersen currents (J_P) implying an equatorward electric field driving this E-FC,
- the earthward Poynting flux ($S_{||}$) locally maximized to ~20 mW/m^2 implying dayside magnetopause reconnection related energy deposition.

DMSP-F13 detected particle precipitation regimes:
The earthward Poynting flux maximized within this E-FC appearing in the llbl regime but not within the cusp regime that was outside this E-FC.

31 August 2005; DMSP 13: 23.40-23.84 UT

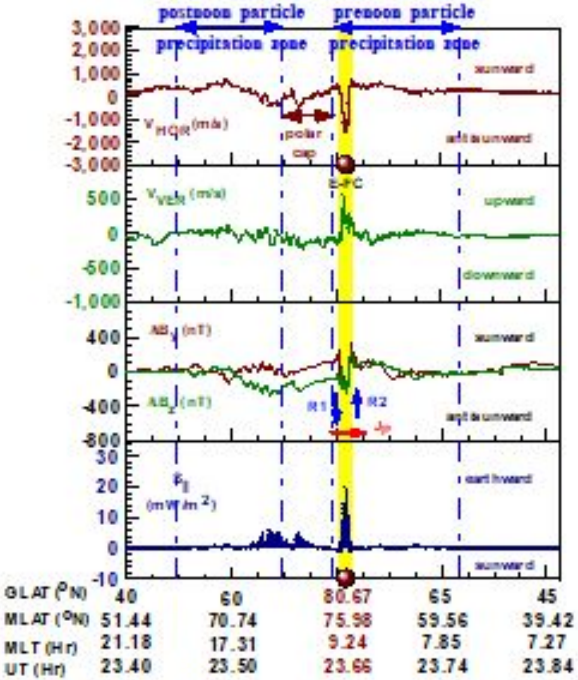

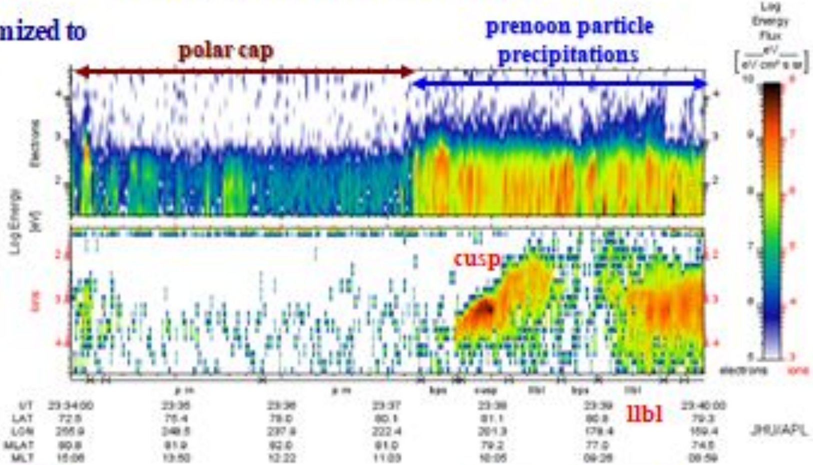

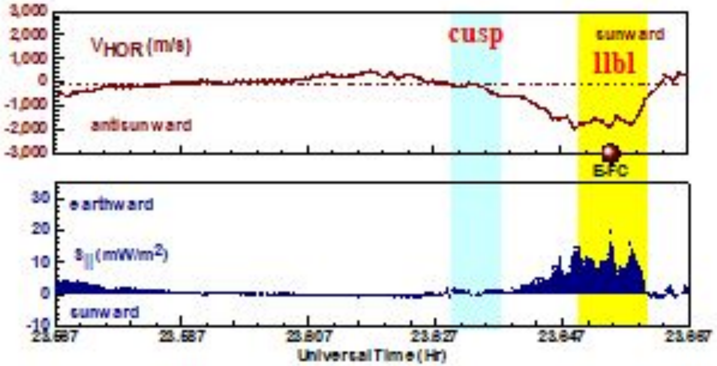

OpenGGCM simulations for the eastward flow channel (E-FC) event detected by DMSP-F13 at 2339 UT on 31 August 2005:

OpenGGCM simulated dissipated Joule heating rate (W_{diss}; W/m^2) at 2339 UT :

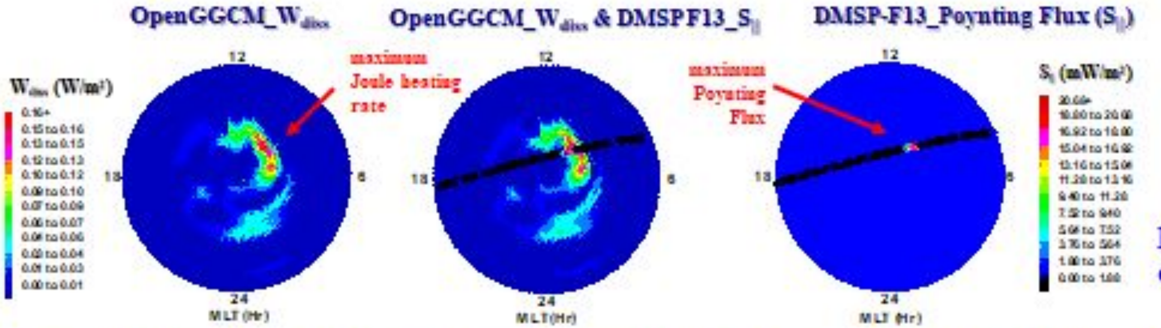

OpenGGCM simulated dissipated Joule heating rate (W_{diss}) correlates well with the DMSP-F13 detected earthward Poynting Flux ($S_{||}$).

OpenGGCM simulated field-aligned currents ($J_{||}$; $\mu A/m^2$) and horizontal drift velocities (V_{HOR}; km/s) at 2339 UT :

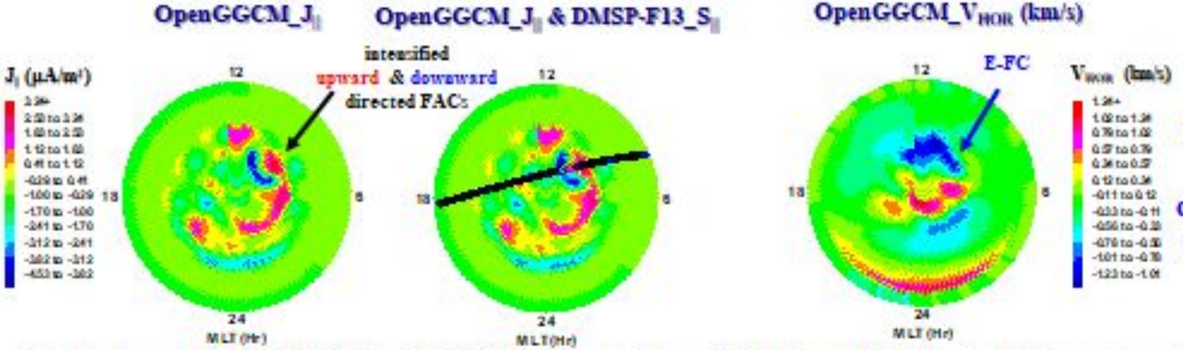

OpenGGCM simulated FAC ($J_{||}$) pattern and E-FC correlate well with those detected by DMSP-F13.

Conclusions: These CHAMP and DMSPF13 scenarios and the OpenGGCM simulations generated for the DMSP-F13 scenario demonstrate the good performance of OpenGGCM depicting dayside magnetopause reconnection and related earthward energy deposition. Thus, OpenGGCM was quite successful in reproducing the various M-I-T coupling processes underlying the development of localized neutral density enhancement.

Meghan Burleigh, UM

ISINGLASS B

Initial conditions are important!

GEMINI-TIA input conditions:

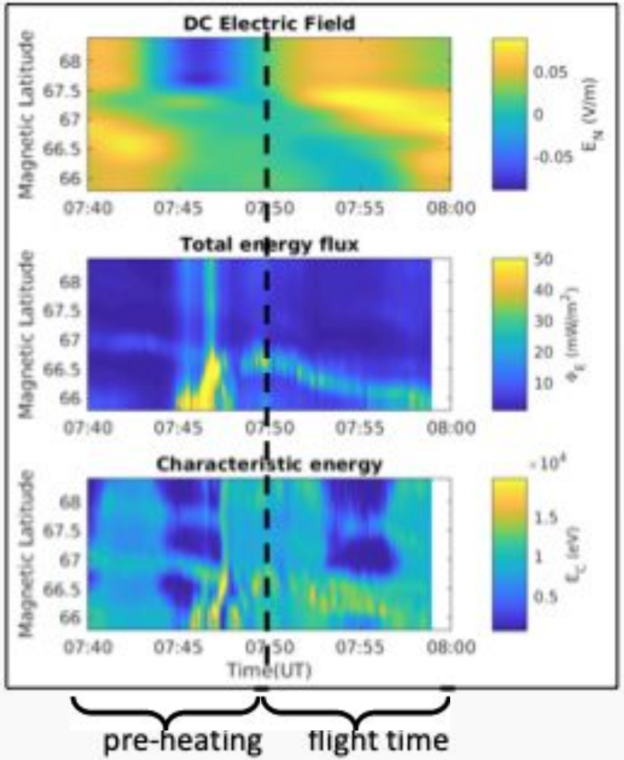

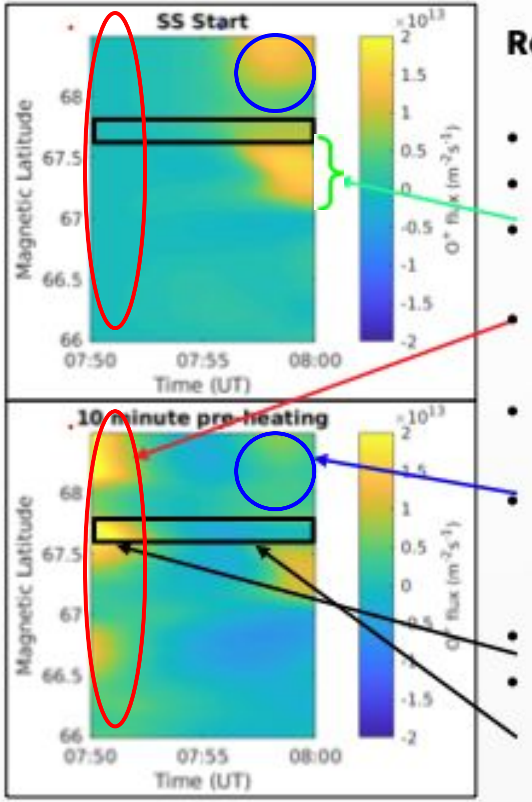

Resulting O+ flux at 1000 km: (minus background):

- Upflows reach alt. in ~4 mins.
- DCE generates strong upflows
- Auroral arc drift "spreads" the upflow region
- Pre-heating effects from dynamic initial conditions
- Pre-heating significantly modifies the ion response
- Much of the ion source population has been already uplifted resulting in a smaller responses to DCE
- O+ flux from shear driven upflow
- The shear end results in downflow that overcomes subsequent upflow from DCE

Influence of initial conditions

E-region impacts:

- Shown at 125 km
- Electron impact ionization increases local densities
- Within 2 minutes, density differences are within 4%
- **Pre-heating has minimal influence**

F-region impacts:

- Shown at 310 km
- DCE drives density cavities through temperature sensitive chemistry
- Density differences >35% persist to end
- **Pre-heating has a lasting influence**

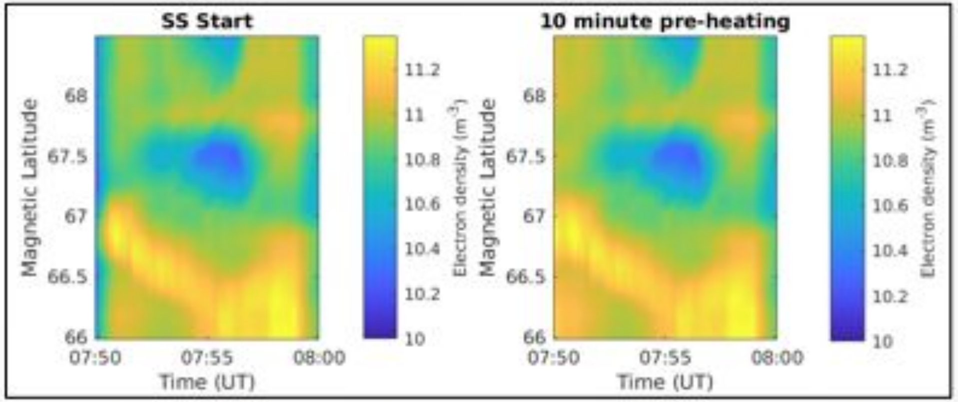

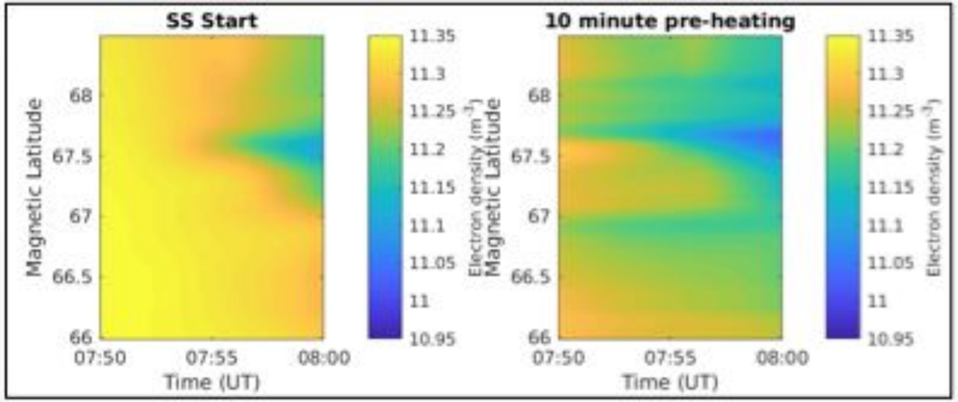

Where is the upflow… really?

Realistic spatiotemporal variability is important when accurately determining the location and amount of upflow and potential outflow to the magnetosphere.

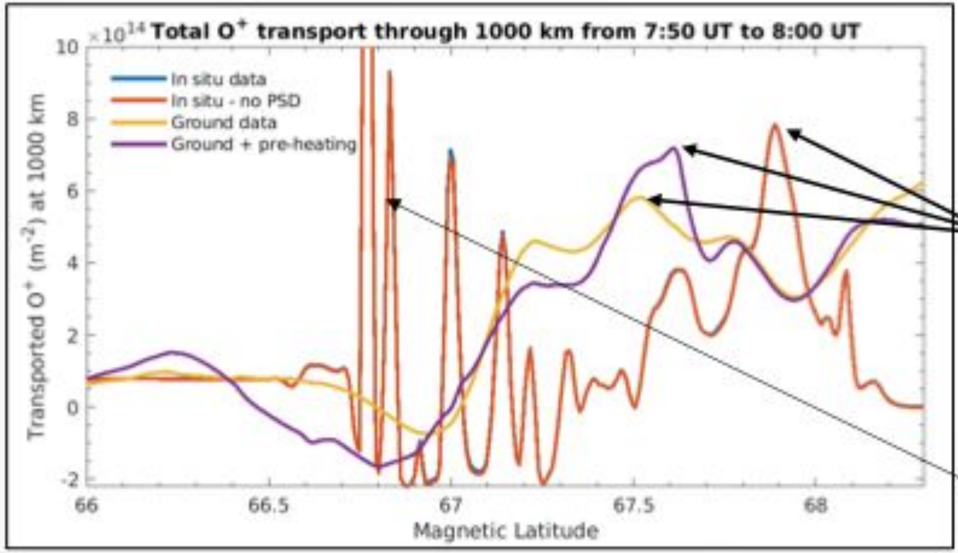

The location of maximum O^+ transport is dependent on energy source variability.

Artificially stable DCE structures in the rocket data-driven simulations overestimate the total number of O^+ ions.

Rachel Frissell, NJIT

ULF Wave Measurements from the Antarctic Polar Cap

Andrew Gerrard, Rachel Frissell, Kevin Urban
Center for Solar-Terrestrial Research - NJIT

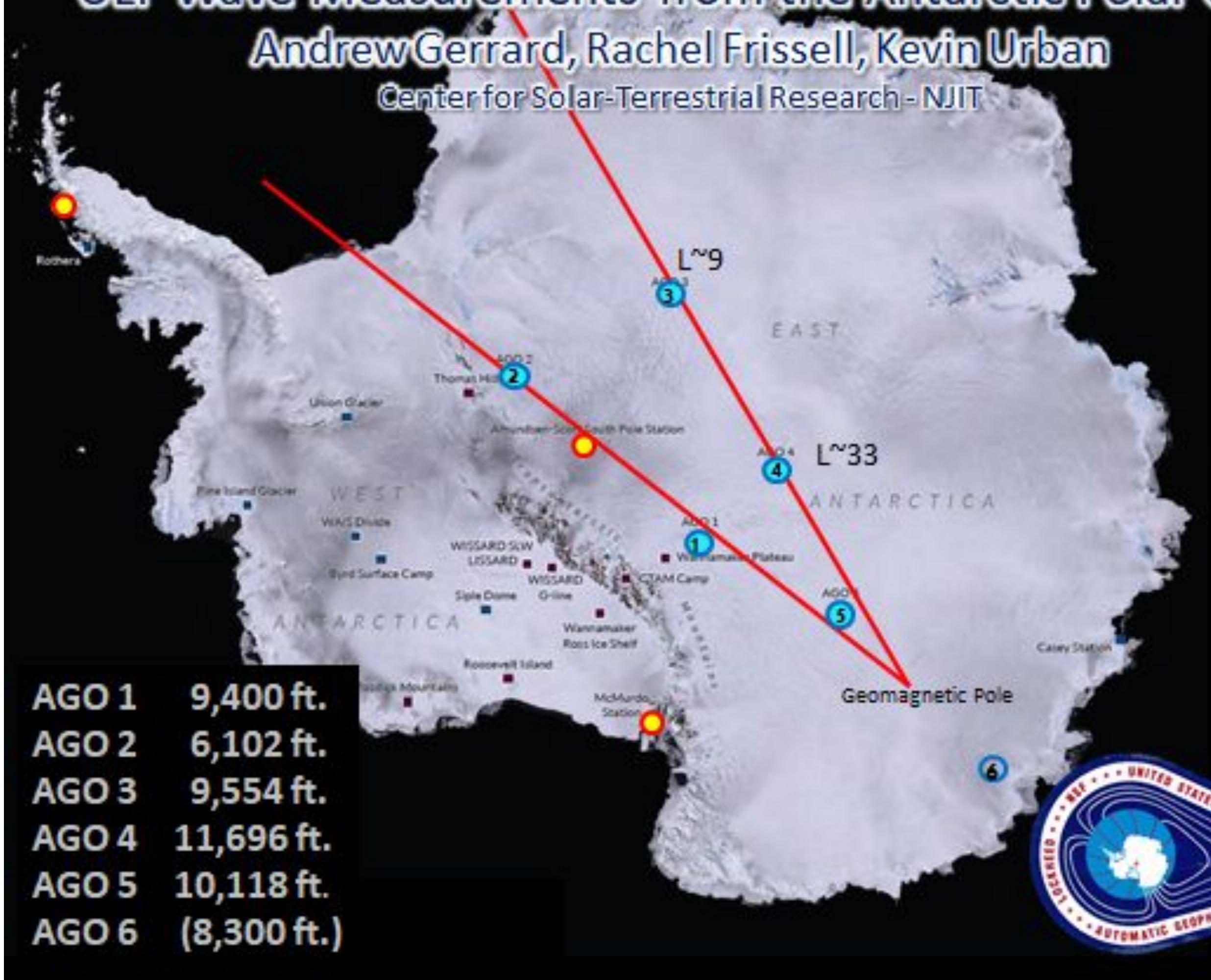

AGO 1	9,400 ft.
AGO 2	6,102 ft.
AGO 3	9,554 ft.
AGO 4	11,696 ft.
AGO 5	10,118 ft.
AGO 6	(8,300 ft.)

Solar Wind ULF Coupling Into the Polar Cap

AGO2 Climatology

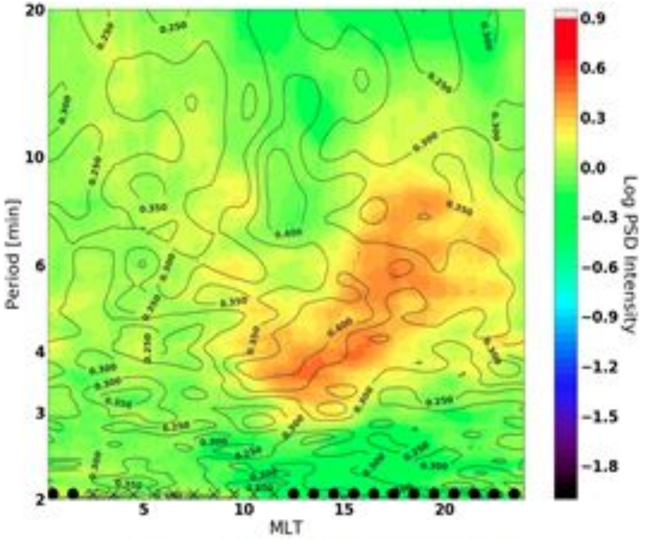

"In-direct solar wind ULF influence"

AGO5 Climatology

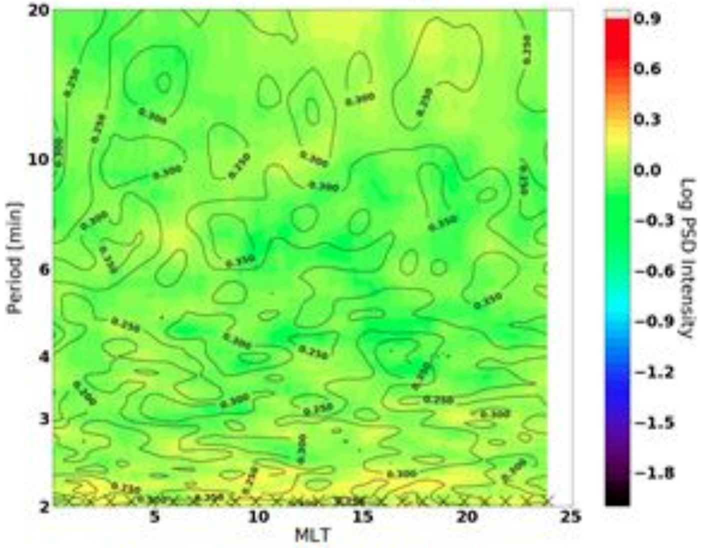

"Direct solar wind ULF influence"

- ULF climatologies demonstrated last year in Frissell et al., 2018 GEM-CEDAR poster
- Nightside ULFs correlate to injection-driven drift-mirror instabilities, e.g., Cohen et al. [2016], Cooper et al. GEM2019 Poster, Soto-Chavez et al. [2019]
- ULF features seen AGO5 are directly related to solar wind ULFs (e.g., Urban et al. [2016])

Magnetospheric ULF Coupling Into the Polar Cap

"What do we do for solar wind measurements without ACE? I want to replace it."

-Kevin Urban, AGU 2015

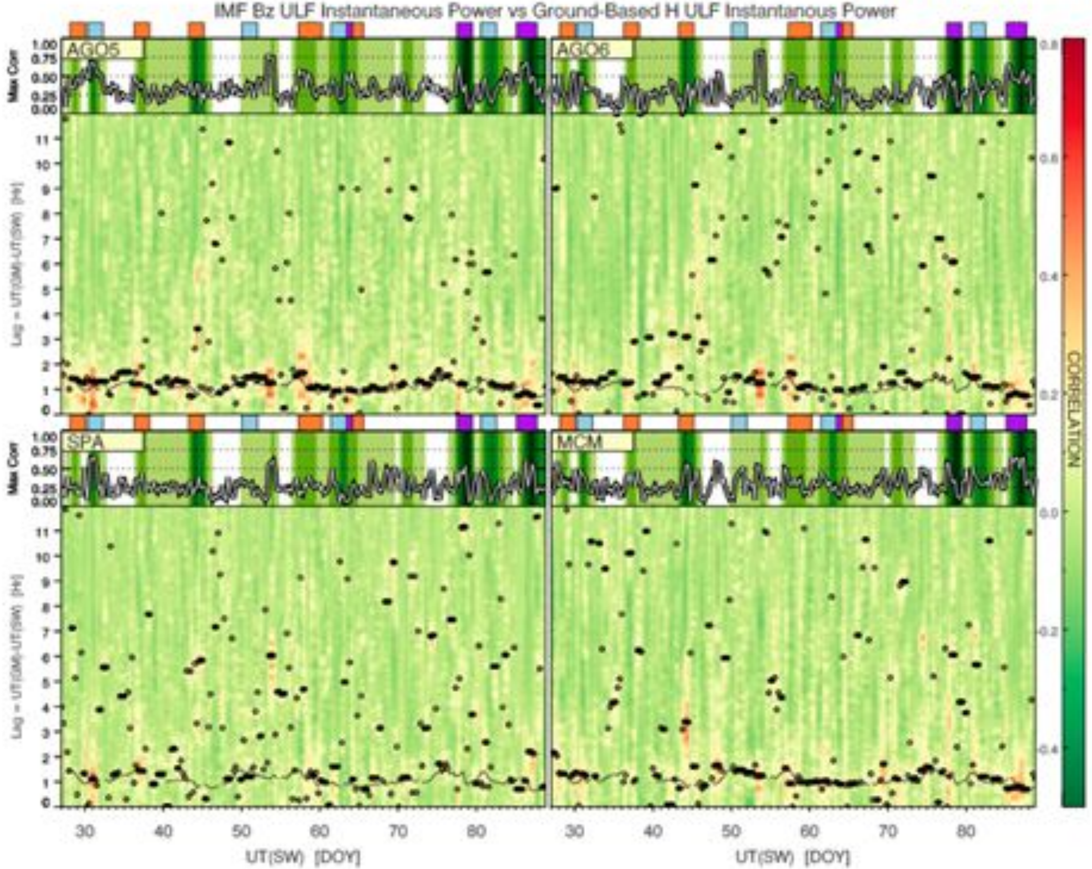

Ashton Reimer, SRI

Summary:

- New low duty cycle capability for RISR-N due to installation of 200kW generator (NSF!)
- Nearly 24/7 continuous multiple beam operations since April 17, 2019 and operations are still going (64 days)!
- 57 days of data shown here contains:
    - 2 CMEs: 11 and 14 May, 2019
    - structured convection before, during, and after CMEs
    - F region density depletion associated with ion temperature enhancements during CMEs (outflow?)
- How do we best exploit low duty continuous measurements at RISR?

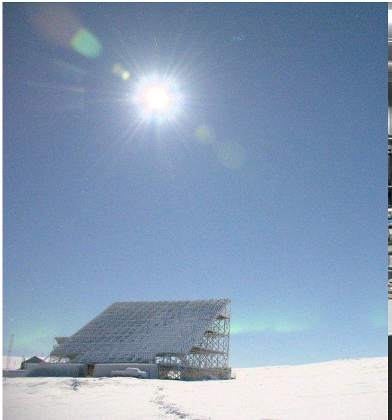

Electron Temperature: 0 to 5000 K

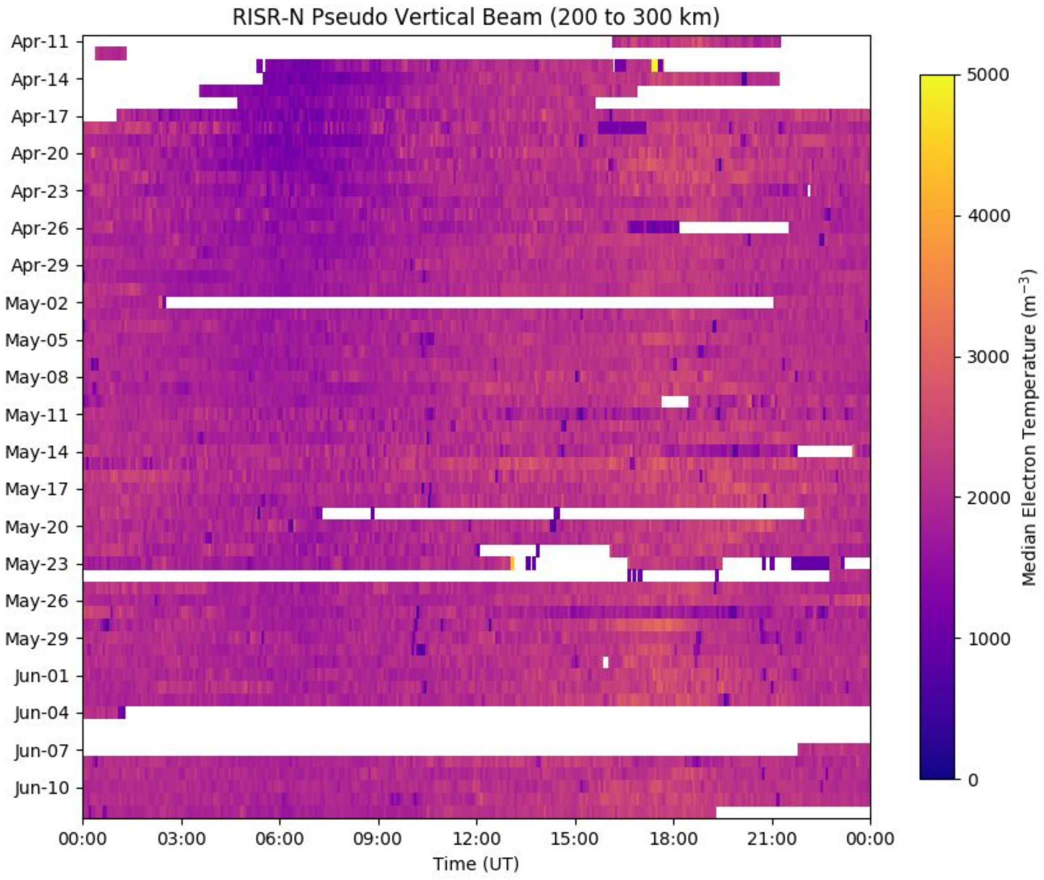

Electron Density: 1e9 to 5e11 m^-3

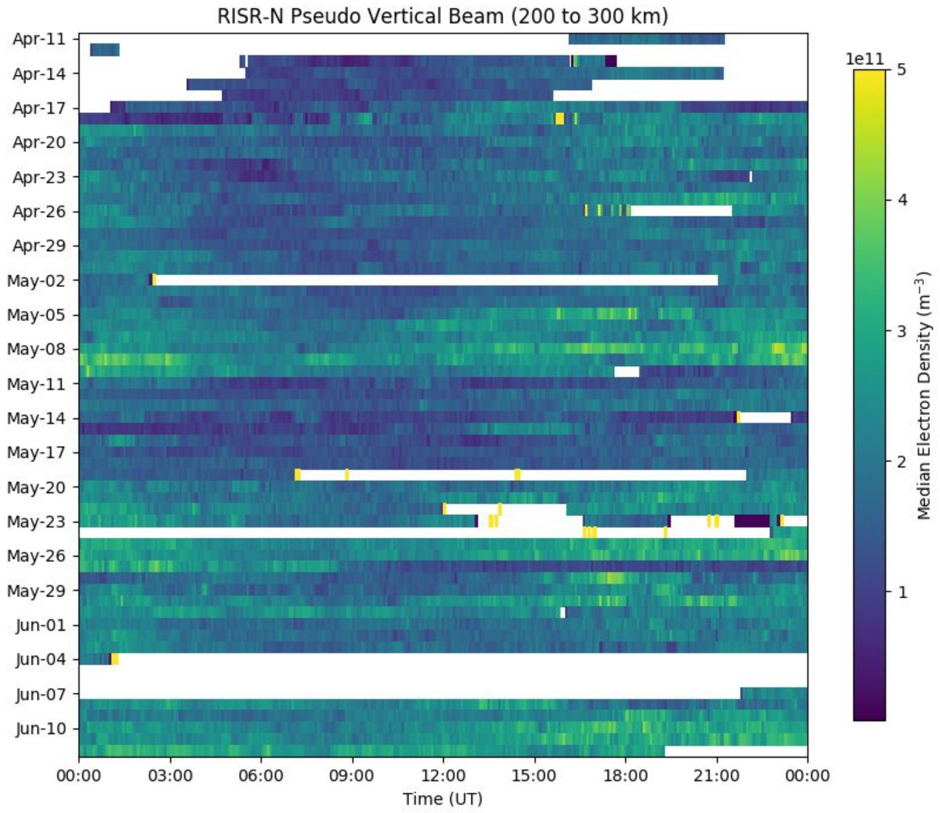

Ion Temperature: 0 to 2500 K

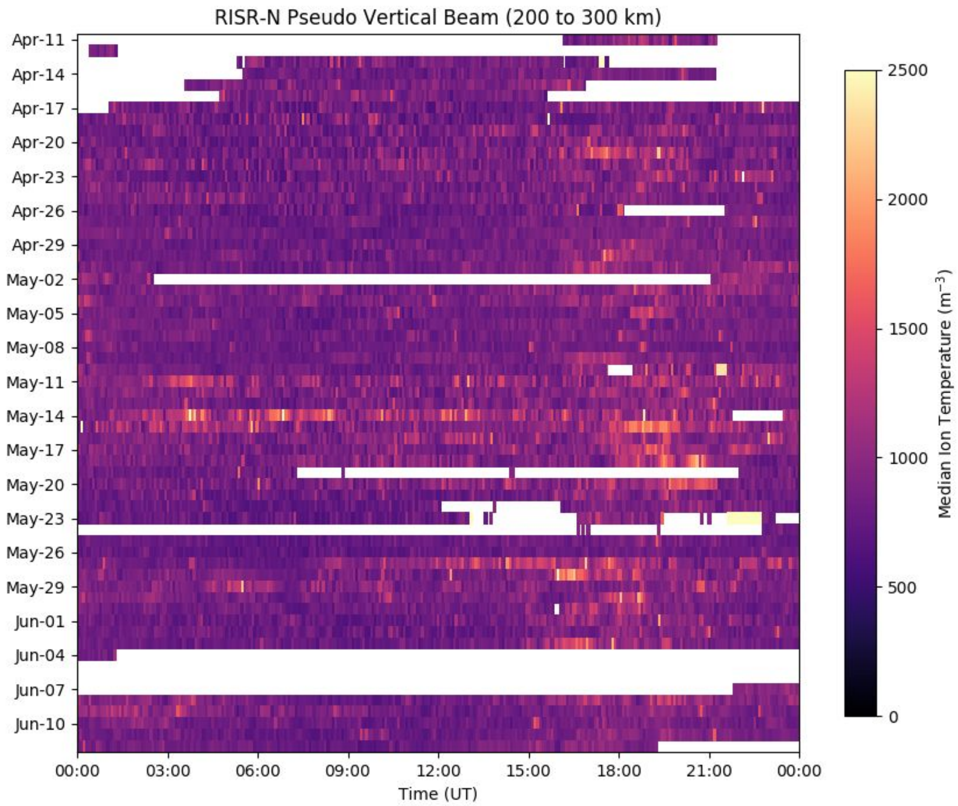

CME arrivals: May-11 and May-14

Convection Velocity East Component

Convection Velocity North Component

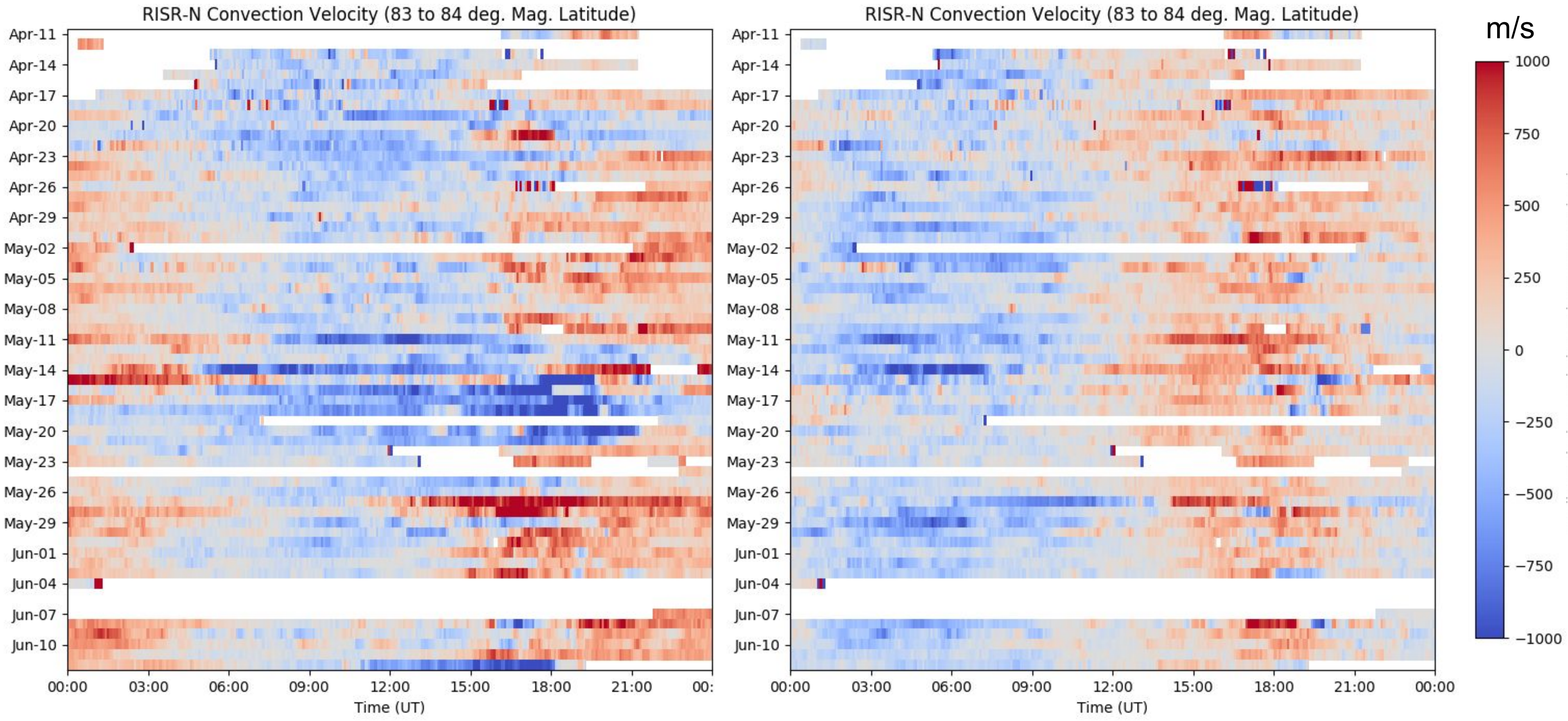

Nathaniel Frissell, NJIT

HF Antarctic Receiver

Nathaniel A. Frissell[1], Robert Melville[1], Andrew Stillinger[1], Gil Jeffer[1], Andrew J. Gerrard[1], and Philip J. Erickson[2]
[1]New Jersey Institute of Technology [2]MIT Haystack Observatory

Objective: Study ionospheric variability with
- HF signals of opportunity
- Low-cost/Hobby Equipment (Citizen Science Access)

Equipment:
- Red Pitaya 125-14
  - HPSDR Emulator Software
  - GNU Radio
  - MIT Haystack DigitalRF
- Raven Single Board Computer (SBC)
- GPS for Time Stamping
- 1 TB Ruggedized SSD
- DXE RF-PRO-1B Active Mag Loop
  - 0.1 - 30 MHz
- 120 W 32V Solar Panel
- AGO Batteries

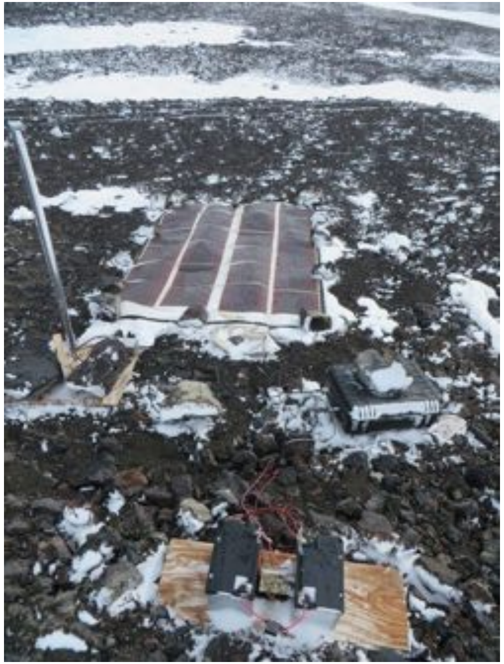

HF Antarctic Receiver

- Record Raw IQ Voltages
- 6 Bands 48 kHz Bandwidth
    - CHU, Ottawa, Canada
    - HF Ham Radio
    - 3, 7, and 14 MHz

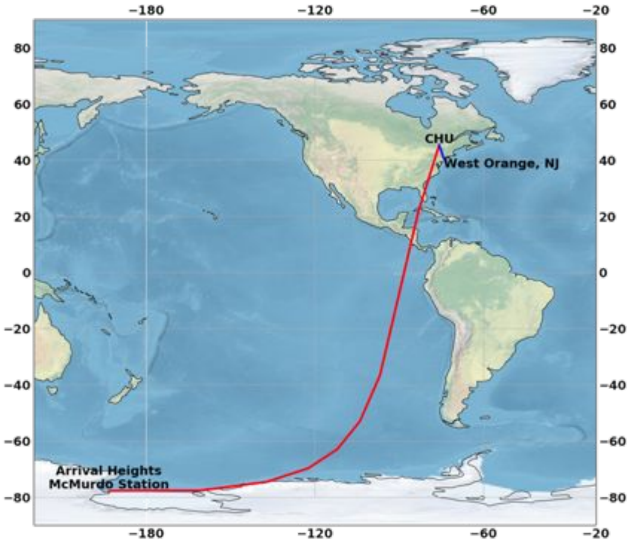

7 January 2019

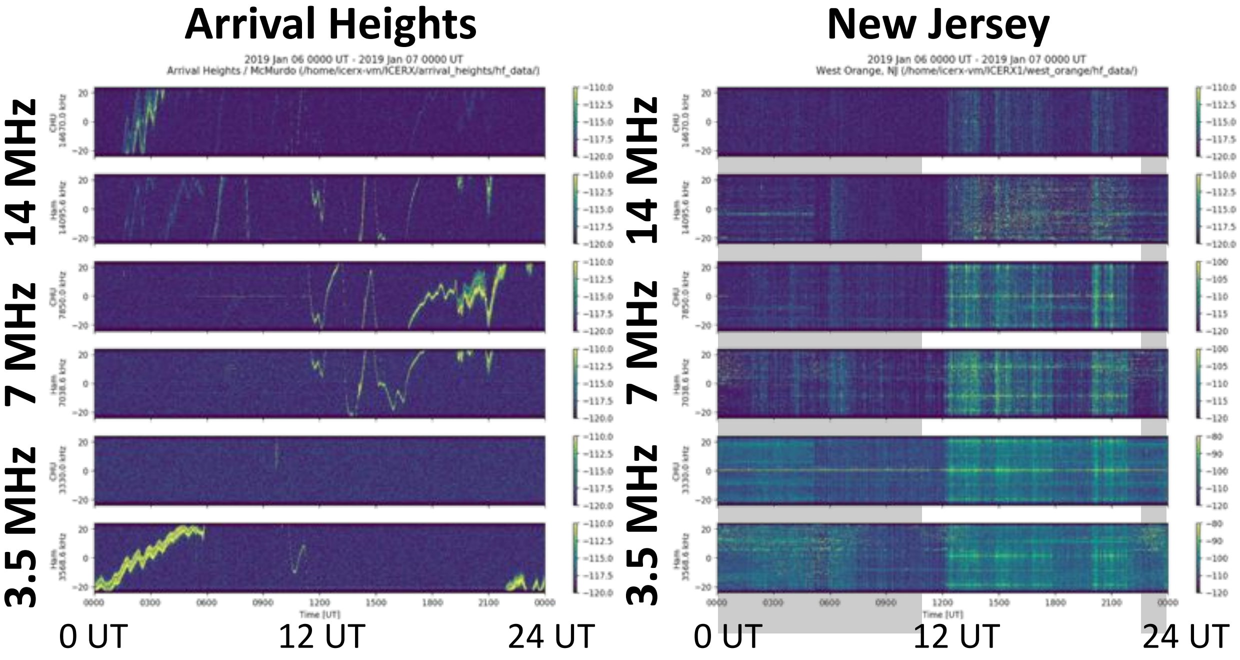

HF Antarctic Receiver

7 January 2019

CHU @ Arrival Heights | **CHU @ New Jersey**

14 MHz

7 MHz

3.5 MHz

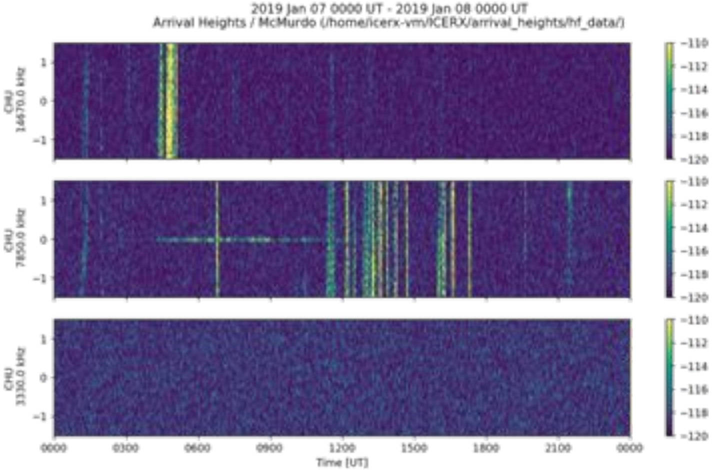

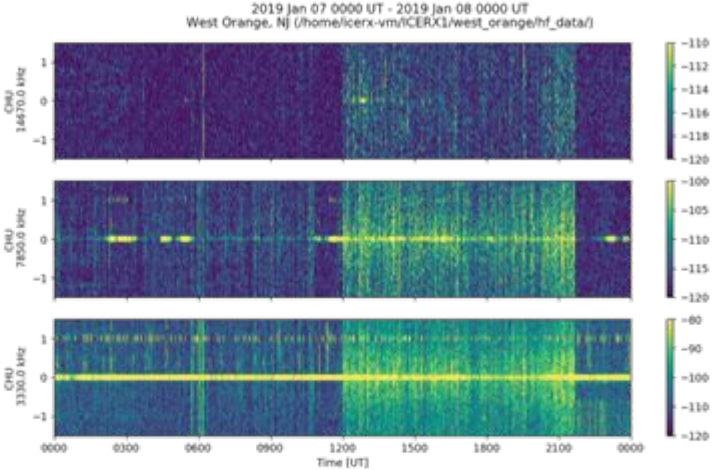

0 UT 12 UT 24 UT 0 UT 12 UT 24 UT

Alex Chartier, JHU/APL







RadioICE: A New HF Ionospheric Sounder in Antarctica


Alex Chartier, **Ethan Miller**

CEDAR 2019, Santa Fe NM



Acknowledgements
NSF AGS-1341885, OPP-1643773





Motivation

- F-region density enhancements seen using Swarm in 2014-2018 [*Chartier et al.* 2018]
- Southern hemisphere **totally opposite** expectations (expected NH pattern shifted by six months)
- Need to validate from ground-based perspective

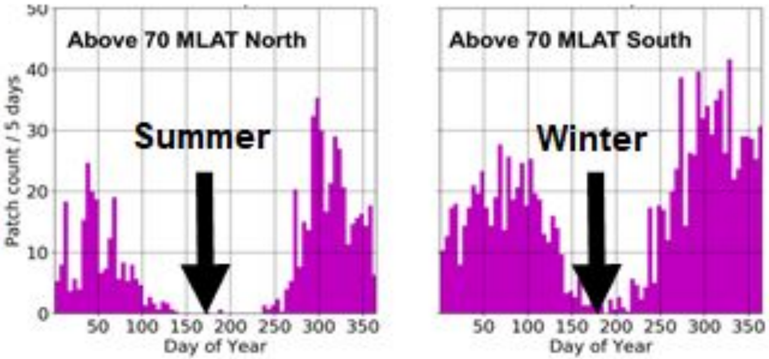

Experiment (tech demo)

Parameter	Spec
Duty Cycle	100%
Tx. Power	5 W (current) - 100 W (March)
Freq. Range	2.6-16 MHz (12 discrete freqs)
Cadence	1 minute frequency revisit
Range	6000 km unaliased @ 6 km res.
Bandwidth	50 kHz
Emission	BPSK (Gaussian p.r. code)
Doppler	500-5000 m/s @ 2 - 15 m/s res.
Data usage	5 MB/s, 1.4 kB/received echo
Cost	550 k

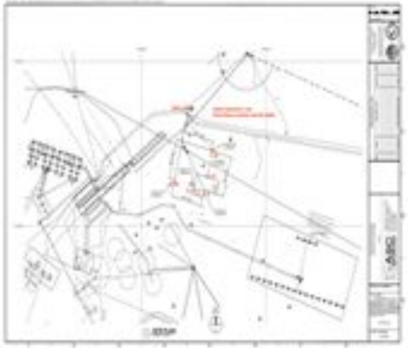

February 2019: Bistatic, multi-frequency HF sounder installed at McMurdo (Tx) and South Pole (Rx)
System identifies F-region density enhancements in the southern polar cap

Results

12 frequencies from 2.6-16 MHz (only showing those with returns)
Cadence: 1-minute
Range res: 6 km
Tx power: ~100 watts.

vHt: Virtual height (assumes mirror reflection at midway point between McMurdo and South Pole & 3E8 m/s group velocity)

McMurdo is at UTC + 12

- Consistent E-layer on 5 MHz, occasionally 6 MHz.
- Sporadic F-layer on 5-7 MHz occasionally in February, frequently in March, usually local afternoon
- F-layer multipath occurs frequently – up to 500km range spreading visible
- Absorption prevalent at frequencies <5 MHz
- Largest range returns at 5.1 MHz

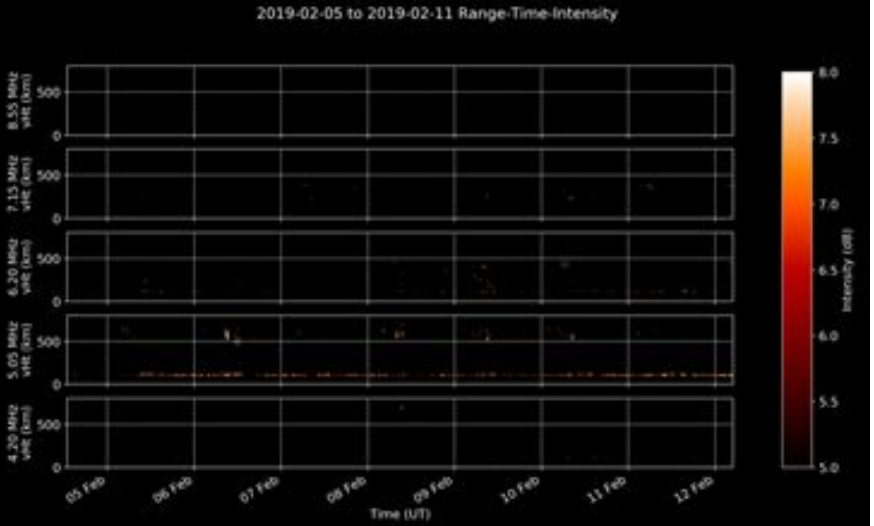

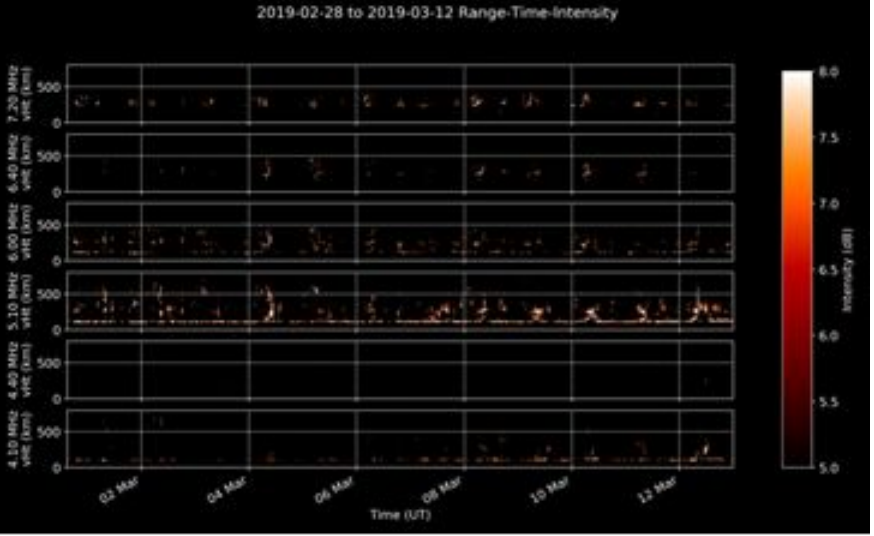

Fall AGU Session: SA014 Pathways of Dynamic Magnetosphere Coupling to High-Latitude Ionosphere

Olga P Verkhoglyadova, Cheryl Y Huang, Michael Hartinger and Stephen R. Kaeppler

Magnetosphere-ionosphere (MI) coupling is one of the most important science topics for the near-Earth environment and space weather. Recent observational findings indicate that the MI coupling is inherently dynamic and occurs at multiple spatial scales. Understanding magnetospheric coupling to different ionospheric regions calls for innovative theoretical approaches and combined analysis of multiple datasets. We will re-examine the roles of possible coupling pathways (large and mesoscale fields, particles and ULF waves). How are these coupling mechanisms incorporated in drivers of physics-based models? What are the effects of coupling at different ionospheric altitudes and regions? How to quantify energy transport? How various precipitating particle populations contribute to local ionospheric conductivity? What is the role of ULF waves in MI coupling at different altitudes? What is the impact of the ionospheric feedback instability? Discussions of multi-instrument observations, including satellite conjunctions, ISR, SuperDARN, magnetometer chains, rocket measurements, and of modeling efforts are solicited.